STRESS WAVES IN TEST SPECIMENS DUE TO SIMULATED ACOUSTIC EMISSIONS

Thesis for the Degree of Ph.D.

MICHIGAN STATE UNIVERSITY

Robert J. Kroll

1962

This is to certify that the

thesis entitled

STRESS WAVES IN TEST SPECIMENS
DUE TO
SIMULATED ACOUSTIC EMISSIONS

presented by

Robert J. Kroll

has been accepted towards fulfillment
of the requirements for

Ph.D. degree in Applied Mechanics

Clement A. Tatro
Major professor

Date 7/25/62

O-169

ABSTRACT

STRESS WAVES IN TEST SPECIMENS
DUE TO
SIMULATED ACOUSTIC EMISSIONS

by Robert J. Kroll

When a test specimen is loaded, acoustic emissions occur at various strain levels. These acoustic emissions create very small stress waves in the test specimen. These stress waves are detected using a piezoelectric crystal at the end of the test specimen. However, the signal from the piezoelectric crystal is very complicated and difficult to interpret.

The purpose of this investigation is to determine an optimum system design, which consists of the specimen, the electronic instrumentation and the experimental technique, for the study of acoustic emissions.

Natural acoustic emissions create extremely small amplitude stress waves. Therefore, in this study the acoustic emission is simulated by burying a small piezoelectric crystal in an enlarged version of the test specimen. The simulated acoustic emission is similar in character to the natural emission, but its amplitude is much larger.

The nature of the stress wave propagation through the specimen is determined analytically and verified

experimentally.

The knowledge of the stress wave propagation allows an optimum specimen design to be postulated. An experimental investigation verifies that this specimen design cleans up the signal from the crystal.

The optimum specimen design is used in a system in which the electronic instrumentation and the experimental techniques are varied. Several different systems are found which produce an acceptable output signal for acoustic emission research. This output consists of a relatively large amplitude and short duration pulse, followed by lower amplitude "hash".

A recommendation of an optimum system design for the study of acoustic emissions is given.

Analytical and experimental studies are conducted to establish the validity of using a simulated acoustic emission source and an enlarged test specimen.

STRESS WAVES IN TEST SPECIMENS DUE TO SIMULATED ACOUSTIC EMISSIONS

By

Robert J. Kroll

A THESIS

Submitted to
Michigan State University
in partial fulfillment of the requirements
for the degree of

DOCTOR OF PHILOSOPHY

Department of Applied Mechanics

1962

ACKNOWLEDGEMENTS

I wish to express my gratitude to Dr. Clement A. Tatro for suggesting the research problem of this dissertation and for his encouragement and valuable guidance as my research advisor. I also wish to thank Dr. Lawrence E. Malvern for his assistance with certain aspects of the analytical work.

I appreciate the services of Mr. Don Childs and Mr. Richard Jenkins of Michigan State University and Mr. Frank Busher and Mr. Harry Fryer of the University of Cincinnati in the fabrication of the test specimens.

I wish to thank all of the members of my guidance committee for their help and encouragement.

My special gratitude is extended to the National Science Foundation for their twofold assistance. First, for the Science Faculty Fellowship, which made this entire dissertation possible. Secondly, for the extensive electronic instrumentation which they provided through an acoustic emission research grant under the supervision of Dr. Tatro.

I.

II.

III.

TABLE OF CONTENTS

I. Introduction 1

II. Description of Experimental Techniques 8

A. Discussion 8

B. Specimen Geometries 8

C. Simulated Acoustic Emission Input 11

D. Crystal Pickup of the Stress Wave 16

E. Amplification of the Signal from the Crystal Pickup 18

F. Filtering the Amplified Signal from the Crystal Pickup 19

G. Monitoring and Recording the Output Signal 20

H. Frequency Response of the ADP Crystals 21

III. Analytical Prediction of the Modes of Stress Wave Propagation 31

A. Discussion 31

B. Mathematical Presentation of the Acoustic Emission Source 33

C. Stress Wave Propagation in the Test Section 35

D. Stress Wave Propagation in the Transition Sections 37

E. Stress Wave Propagation in the Cylindrical Outer Sections 39

F. Stress Wave Propagation in the End Sections 39

G. Stress Wave Propagation in the Entire Specimen 41

H. An Optimum Specimen Design Based on the Theory 48

I. Theory of Steel End Caps for the Specimen 50

TABLE OF CONTENTS (CONT.)

IV. Experimental Verification of the Modes of Stress Wave Propagation 56

A. Discussion 56

B. Response of an ADP Crystal to a δ(t) Impulsive Stress Wave 57

C. Effect of Filtering 62

D. Effect of the Condition of the Grease Seal 63

E. Effect of the Steel End Caps 65

F. Dynamic St. Venant Principle Used in Test Section 66

G. Stress Waves in the Transition Section 68

H. Stress Wave Propagation in the Cylindrical Outer Section 68

I. Stress Wave in the End Section 71

J. Reflections at Critical Points of the Specimen 72

K. Optimum Design of Specimen 75

L. Scale Effects 76

M. Optimum Design of Instrumentation and Experimental Techniques 77

V. Conclusions and Recommendations 79

VI. Bibliography 83

LIST OF FIGURES

1. Geometry of the Test Specimens 86

2. Block Diagram of the Experimental Setup 9

3. The Large, Medium, and Small Size Test Specimens 87

4. Separate Components of the Test Specimens 87

5. Barium Titanate Input Probe 87

6. Experimental Setup for Frequency Response Tests 83

7. ADP Crystal and General Radio Amplifier 87

8. Part of the Experimental Setup for Test Specimens 83

9. The Pulsed Oscillator 87

10. Block Diagram of Frequency Response Tests 24

11. Circuit Diagram for the Pulsed Oscillator 25

12. Frequency Response Curves 28

13. Oscilloscope Records of Frequency Response Tests 89

14. Specimen Geometry 42

15. Stress Waves Associated with a Steel End Cap 54

16. Comparison of the Stress Waves that Excite the ADP Crystal and Return to the Specimen with and without Steel End Cap 54

17. ADP Output Signal before "Cleaning Up" 90

18. Response of ADP Crystal to $\delta(t)$ Impulsive Stress Wave 60

19. Effect of the Grease Seal 64

20. Effect of the Steel End Cap 89

LIST OF FIGURES (CONT.)

21. Test Setup for Cylindrical Outer Section 69

22. Stress Waves in the Cylindrical Outer Section 89

23. Reflection Test Specimen 72

24. Reflected Stresses in Specimen 73

25. Comparison of ADP Crystal Output for Specimens L1, L2, L3 89

26. ADP Crystal Output for Specimen M1 90

27. ADP Crystal Output for Various Instrumentation and Experimental Technique Methods 90

A1. Geometry of the Transition Section 91

A2. Free Body Diagram of an Element of the Transition Section 92

A3. $\delta(t)$ 94

A4. $\delta'(t)$ 94

A5. $\delta(t)/\delta'(t)$ 95

B1. Stress Waves due to a Unit-Step Function Impulsive Loading 98

LIST OF APPENDICES

A. Propagation of $\delta(t)$ Type of Impulsive Stress Wave through a Transition Section 91

B. Stress Wave Propagation in a Half-Space with an Impulsive $\delta(t)$ Load on a Circular Area of the Surface 93

C. List of Electronic Equipment Used in This Investigation 102

LIST OF SYMBOLS

Symbol	Definition
a	radius of a rod
A	cross sectional area
D	diameter**
D_c	diameter of end section*
D_m	diameter of cylindrical outer section*
D_t	diameter of test section*
E	modulus of elasticity
F	length of transition section*
L	length of test specimen*
L_e	length of end section*
M	length of cylindrical outer section*
R	radius of curvature of transition section*
T	length of test section*
t	time
t_s	thickness of steel end cap
u	displacement in the x or ξ direction**
$u(t)$	unit step function (see Appendix B)
$U(\xi)$	displacement function of ξ only**
v_b	bar velocity
v_d	dilatational wave velocity
v_s	shear wave velocity
x	axial coordinate**
γ	a parameter measuring the taper of the transition section**

Symbol	Definition
$\delta(t)$	impulse function (see part III B)
ε	strain**
λ	Lame constant
μ	Lame constant
ξ	non-dimensional x coordinate**
ρ	mass density
ρv	acoustic impedance
σ_i	incident stress wave amplitude
σ_r	reflected stress wave amplitude
σ_t	transmitted stress wave amplitude
ω_R	end resonance natural frequency for a bar

Subscripts

o	property at x = 0 **
1	upstream property
2	downstream property

---

* See Figure 1

** See Appendix A

I

INTRODUCTION

The ever-increasing demands of modern technology upon structural materials have required that new materials be developed which have higher strength per unit weight and can withstand extremely high stresses and severe environments. In the past, advances in material development have been accomplished mainly through chemical technology. It now appears that further advances will only be achieved through developments in the fundamentals of solid state physics.

The theory of dislocations, which was originated in 1934 by Taylor (TA 34)* and Orowan (OR 34), plays an important role in the modern solid state physics of materials. If it were not for the presence of imperfections in crystals, such as dislocations, theoretically structural materials would be approximately 100 times as strong as they actually are (CO 53). The theory of dislocations explains why materials are so weak. Macroscopic strain, especially in the plastic range, can be shown to be a function of the motion of the dislocations in the material (JO 59). Therefore, a fundamental knowledge of the properties of dislocations is essential for advancement of the material sciences.

---

* Refers to the Bibliography.

One of the lesser known properties of dislocations is "acoustic emission". The first investigation of acoustic emission was made in Germany by Kaiser (KA 50) in 1950 as a doctoral thesis. There are audible sounds, known as "tincry", generated when tin is handled or worked. This led Kaiser to investigate whether other materials produce non-audible acoustic sounds when they are deformed. He found that very low amplitude acoustic emissions, which could only be detected using very sensitive electronic equipment, were produced during the process of tensile testing of a specimen. These acoustic emissions were believed to be due, in part, to the motion of dislocations.

As in all pioneering efforts, Kaiser's investigations left many questions unanswered and stimulated others to research activities in this area. In the United States, B. H. Schofield of Lessells and Associates in Boston, Massachusetts and C. A. Tatro of Michigan State University, each became interested in acoustic emission research because of Kaiser's work. Independently, each initiated a research program, whose first objective was to verify Kaiser's findings.

During 1955, Schofield (SC 58) found that he could not verify some of Kaiser's results. Specifically, although he found that an acoustic emission phenomenon did exist, he could not agree with Kaiser's conclusion that

"th
pre
the
not

"there exists a characteristic distribution of the frequency and amplitude spectrums which is related to the stress level within the material and the past metallurgical history of the material."

Both Schofield and Tatro found that the signals received during acoustic emission experiments were rather complicated and were hard to identify as being caused by an acoustic emission from the material in the critical cross section of the test specimen. The shape of the specimens used in their experiments was roughly as shown in Figure 1. An acoustic emission, which originates inside the test section, T, at the center of the specimen, certainly will be distorted seriously and reflected many times before it arrives at the detector, which is located at one end of the specimen (surface A). The question now becomes how to interpret the received signals in terms of the acoustic emissions generated within the specimen. Any further meaningful research depends on the resolution of this problem.

In 1959, Schofield (LE 59) made a limited attempt to find the stress wave propagation through specimens of this type. He introduced stresses at one end of the specimen and detected them at the other end. Not much insight can be gained by this experiment because the

sha

pic

fre

fou

dis

wav

spe

to

num

par

Dur

for

vol

cou

of

wa

Dr.

mo

fr

wa

to

Th

to

shape of the specimen is complicated and, therefore, the pickup signals are complicated. He found "sensitive" frequencies of the specimens and at other frequencies he found mostly hash. The reasons for this behavior will be discussed in part II H. The question of how the stress wave caused by an acoustic emission propagates through the specimen was not completely resolved by his work.

Tatro, in his acoustic emission research from 1956 to the present time, has attempted to correlate the number of acoustic emissions, which occured at various parts of the stress-strain curve, to the onset of yield. During this work, he determined that there is a need for a more fundamental understanding of the process involved in stress wave propagation through the specimen caused by the occurrence of acoustic emissions. Because of this need, the research presented in this dissertation was initiated by the author under the supervision of Dr. Tatro.

The purpose of this research is to determine the mode of stress wave propagation in the specimen resulting from natural acoustic emissions. To accomplish this, it was necessary to simulate the acoustic emission source and to use an enlarged specimen. This will be explained below. The knowledge of the stress wave propagation should lead to possible changes in specimen geometry, the attending

electronic instrumentation and the experimental techniques with the aim of optimizing the system used in natural acoustic emission research. This optimization should produce a "clean" signal, which is of the maximum possible amplitude and the shortest duration. This signal will be the evidence of the occurrence of a single acoustic emission. The number of acoustic emissions, occuring during a given time, will be determined by counting these characteristic signals.

As stated previously, the energy in the acoustic emissions is extremely small. In his experimental work Tatro found that the signals from the acoustic emissions, even after large amplification, were often not much larger than the electronic noise in the equipment. At these levels, it would be impossible to perform experiments to determine the stress wave propagation through the specimen.

The experimental setup for studies using natural acoustic emissions is cumbersome and usually involves testing at night to eliminate extraneous "noises". In addition, the acoustic emissions occur at irregular intervals. There are often periods of no emissions followed by a burst of closely spacedemissions.

For these stress wave propagation studies, it is essential that an isolated emission can be initiated at will and observed. Two or more closely spaced emissions

cou

res

be

int

a s

spe

ing

app

ele

amp

len

tes

bec

emi

was

emi

pie

mon

lar

var

of

by

lar

tic

could lead to problems of interpreting the experimental results. Obviously, natural acoustic emissions will not be satisfactory for these studies.

Since the natural acoustic emissions occur in the interior of the specimen, it is necessary to introduce a simulated acoustic emission in the interior of the specimen and not on the surface. This is done by "burying" a small piezoelectric crystal in the specimen and applying an electric pulse to it. The smallest piezoelectric crystal available that would give a reasonable amplitude signal is a cylindrical crystal of 1/16 inch length and diameter. The crystal must be buried in the test section, dimension D_t of Figure 1 of the specimen, because this is the region of the natural acoustic emissions. The specimen designated as S1 in Figure 1 was used by Tatro in his research of natural acoustic emissions. It would be impossible to bury this size piezoelectric crystal in the test section of this specimen. It was decided to use a test specimen five times larger, designated as L1. This specimen geometry was varied slightly (specimens L2 and L3) to study the effects of certain geometry changes. Scale effects were studied by comparing results in two different size specimens; large and medium.

Analytical predictions of the stress wave propagation through the specimen were made. Then experimental

investigations were conducted to verify the analytical predictions. Better specimen designs and methods of instrumentation were deduced based on the analytical and experimental evidence. Of course, a limited number of system designs were investigated, but the design trends are clear.

Finally, recommendations will be made for the design of a system, consisting of specimen, electronic instrumentation and experimental techniques, for natural acoustic emission research.

II

DESCRIPTION OF EXPERIMENTAL TECHNIQUES

A. Discussion

The experimental equipment used in this investigation consists of the test specimens and a system of electronic instrumentation. A block diagram of the experimental setup is given in Figure 2. Figures 3 through 9 contain photographs of the specimens and the electronic instrumentation.

A detailed discussion of the experimental techniques follows.

B. Specimen Geometries

The various test specimens used in this investigation are presented in Figure 1. They are fabricated from 2024 aluminum, which is the material used by Tatro in his research. As mentioned in the Introduction, it is necessary to use specimens which are basically five times larger versions (L1, L2, and L3) of the original test specimen (S1) used by Tatro in his research of natural acoustic emissions. Variations between L1, L2, and L3 are for the purpose of studying the effects of certain geometry changes. The medium size specimen (M1) is studied to determine scale effects. The various sizes of specimen can be seen in Figure 3.

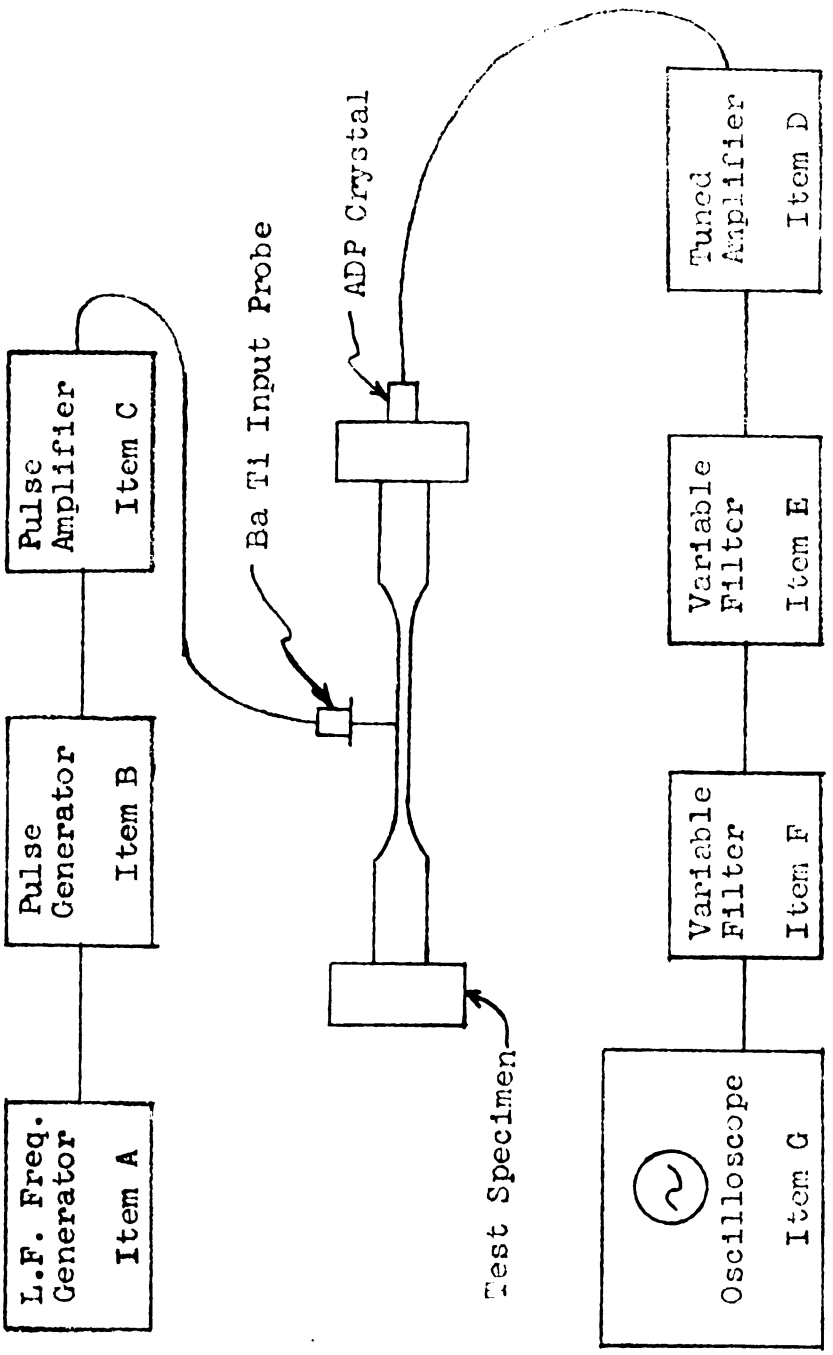

Figure 2. Block Diagram of the Experimental Setup

The specimens in this investigation are all axially-symmetric, that is the cross section is circular at every station along the length. Every specimen has an enlarged end section, because, in studies of natural acoustic emissions, the specimen must be used for testing in a tensile testing machine. The load is applied through bearing stresses on surface B. It is standard practice to put a layer of sound proofing material between surface B and the loading fixture (WO 61).

Every specimen contains a test section, which has the smallest cross sectional area of the specimen. It is the region of highest stress in the specimen and, because of this, the acoustic emissions are expected to be originated there. This is the region that will be used to originate the simulated acoustic emissions.

There are transition sections at both ends of the test section. The purpose of this section is to change the cross sectional area of the specimen rapidly and reduce the stresses correspondingly.

All but two of the specimens have uniform sections between the transition sections and the ends. The purpose of this section is to allow any non-uniformity of the applied tensile stress in the specimen to be smoothed out before the test section. This section is the one that is varied to "clean up" the signal.

The fabrication of these specimens is time consuming

and expensive. For this reason, the three large specimens, L1, L2, and L3, are not three separate specimens. First specimen L1 was fabricated and tested. When this testing was completed, specimen L1 was machined and became specimen L2. Similarly, L3 was made from L2.

Separate component parts of both the large and the medium size specimens were fabricated. These are shown in Figure 4. It is possible to build up portions of the specimens using these components plus uniform rods. These parts are "integrated" by mechanically holding them together and using a thin layer of High Vacuum Grease (manufactured by Dow Corning Corporation) in the joints. This method allowed many specimen geometries to be investigated without the expense and time delay associated with manufacturing many specimens. This method was used to get qualitative data which led to the design of several of the actual specimens. This will be discussed later in part IV H.

C. Simulated Acoustic Emission Input

A small Barium Titanate ($BaTiO_3$) piezoelectric crystal*, which was purchased from Electro-Ceramics, Inc. of Salt Lake City, Utah, was used as the source of the simulated acoustic emissions. The crystal is a cylinder of 1/16

---

*This Barium Titanate transducer is actually a specially processed polycrystaline ceramic. However, it is commonly referred to as a "crystal", and this nomenclature will be used here.

inch diameter and height. The flat ends are the positive and negative electrical terminals.

Barium Titanate was selected because this crystal will be subjected to elevated temperatures during its positioning in the specimen. This will be discussed below. Barium Titanate is a ceramic and is particularly suited to withstand temperature. Also Barium Titanate does not require an external polarization voltage.

This crystal must be buried in the test section of the specimen. The crystal will deform when it experiences an electrical voltage pulse. This deformation will produce a stress pulse in the specimen. It will be shown later that this stress pulse has the form of an impulse.

It is necessary to position the crystal inside the test section accurately and supply an electric pulse to it. This is accomplished by making a crystal input probe, which is shown in Figure 5, as follows:

1) The crystal is fastened to one end of a 1/16 inch diameter brass rod about $2\frac{1}{2}$ inches long using Armstrong A1 cement, which is a non-conductor. The axis of the crystal is perpendicular to the axis of the brass rod. At this stage the crystal is mechanically fastened to the rod, but the two electrical terminals of the

crystal are floating.

2) Next one face of the crystal is electrically connected to the rod by using conducting silver paint (Dupont No. 4817).

3) Then the entire rod, except 1/4 inch of the end away from the crystal and the other electrical terminal of the crystal, is coated with Glyptal varnish, manufactured by the General Electric Company. It is then cured for four hours at 100°C. Glyptal serves as an electric insulator.

4) Next, conducting silver paint is used to make a conducting strip about 1/16 inch wide on the surface of the Glyptal from the other face of the crystal out to about 1/3 inch from the edge of the Glyptal. At this stage, the two faces of the crystal are connected electrically; one to the brass rod and one to the silver paint. It cannot be buried in the specimen, because the silver paint would short out with the specimen.

5) Glyptal is coated over the entire part of the probe that was previously coated with Glyptal except for about 1/4 inch at the end away from the crystal. It is cured again.

6) Next, an Amphenol connector is soldered to the rod to form the hot connection. A short brass strip is soldered to the Amphenol connector and

it contacts the silver paint with a spring action to form the ground.

The details of the input probe may be seen in Figure 5. The input probe is also shown in Figures 3, 6, and 8. The part of the probe inside the specimen, which is not shown in Figure 5, contains the crystal. However, the crystal would not be easily distinguishable because of the relatively thick layers of Glyptal.

The crystal input probe was buried in the specimen as follows:

1) A 1/8 inch diameter hole was drilled into the test section of the specimen to a depth 1/8 inch greater than the radius of the test section. The axis of this hole was radial. Its longitudinal position in the test section depended on the test being conducted.

2) Next, the specimen was heated in the vicinity of the hole using a propane torch with a flame spreader. The hole was then filled with melted Woods Metal, which has a melting point of 153°F. If the flame is removed, the specimen and Woods Metal will cool rapidly and the Woods Metal will solidify. The input probe was inserted into the hole in the required position when the Woods Metal was just above 153°F. The Woods Metal firmly

imbeds the probe in the specimen. If the probe were inserted when the Woods Metal is considerably above its melting point, then the Barium Titanate crystal could become depolarized. The Curie temperature of Barium Titanate is 125°C.

The Barium Titanate crystal can be located at any radial position ranging from the centerline to near the surface and its angular position can be anywhere from axial to transverse. Its longitudinal position can be changed by using different holes. If the probe is removed from one hole and moved to another, the old hole is simply filled with Woods Metal.

Woods Metal was selected because of its low melting point and because its acoustic impedance is close to that of aluminum.

The electrical pulse, which is imposed on the Barium Titanate crystal, is provided by three pieces of electronic equipment, items A, B, and C.* These are shown in Figure 6. They are the three pieces on the right from bottom to top respectively. Items A and B are also shown in Figure 8. A square electrical pulse of 50 volts and having a pulse width of 5,000 microseconds is generated in the Rutherford Pulse Generator, Item B. This pulse is amplified to 300 volts in the General Radio Unit Pulse

---

*See "List of Electronic Equipment used in this Investigation" in Appendix C.

Amplifier, Item C. The pulse repetition rate is 5 per second. This is obtained by using the "Sync Out" from the Hewlett Packard Low Frequency Function Generator, Item A, to trigger the Rutherford Pulse Generator.

The Barium Titanate crystal responds to the rise portion and the fall portion of the square pulse. As will be shown later, the crystal creates an impulsive $\delta(t)$* type stress wave in the specimen at each of these times. The stress wave resulting from the impulse associated with the rise portion is observed. The impulse from the fall portion occurs after the oscilloscope has stopped sweeping. The pulse repetition rate of 5 per second is slow enough that the successive stress waves do not interfere with one another, and fast enough that the signal appears to be constant on the scope. The 300 volt amplitude is sufficient to create easily readable stress waves in the specimen, but 50 volts was found to be marginal.

D. Crystal Pickup of the Stress Wave

The stress wave is monitored at Surface A of the specimen, using an ADP (Ammonium Dihydrogen Phosphate) 45° Z cut piezoelectric crystal. This type crystal is designed for the monitoring of normal stresses. The crystal produces a small voltage signal when it is

---

* See part III B for definition of $\delta(t)$

deformed by the incident stress wave.

Two different size crystals were used: each having a 5/8 inch square cross section and one being 1 inch long and the other 1/2 inch long. Each crystal consists of a stack of 8 plates. The natural free-free frequencies of these crystals are 66 kc for the one inch crystal and 130 kc for the 1/2 inch crystal. The one inch crystal can be seen clearly in Figure 7. It can also be seen in Figures 6 and 8. These crystals were also purchased from Electro-Ceramics, Inc.

The ADP crystal was chosen, because it has a high sensitivity and there are no problems of temperature or size as in the case of the Barium Titanate input crystal. Also an ADP crystal requires no external polarization voltage.

The ADP crystal is held in place on Surface A of the specimen by a thin layer of the High Vacuum Grease mentioned in Section II B. When the axis of the specimen is vertical, and Surface A is therefore horizontal, the crystal has no tendency to loosen or move (even if it is supporting its own weight). When the axis of the specimen is horizontal, and Surface A is therefore vertical, the crystal tends to slide down the surface very slowly, because the grease is in shear.

At the beginning of this investigation, a crystal holder and a steel pressure block were used to insure

that the crystal would not move. These were found to be unnecessary, because, even when Surface A is vertical, it is only necessary to relocate the crystal occasionally. It was also found that the clamp and pressure block changed the natural frequency of the crystal. It will be shown in part IV B that this would be an unfortunate complication.

E. Amplification of the Signal from the Crystal Pickup

The maximum amplitude of the voltage signal from the pickup ADP crystal is extremely small (approximately 1 to 2 millivolts). It is necessary to amplify this signal before introducing it into the oscilloscope. A General Radio Tuned Amplifier, Item D, is used for this purpose and it is shown in Figure 7. It may also be seen in Figures 6 and 8. The gain of this amplifier is adjusted to produce an output signal of approximately one volt or less maximum amplitude. This amplifier has an internal variable filter. The "FLAT" filter frequency, which passes all frequencies between 20 cps and 100 kc, was used in all the experiments.

Notice that the electrical leads from the ADP crystal to the amplifier are very short (about 6 inches long). It is essential to amplify the weak ADP crystal voltage signal before it is introduced into a relatively long (about 2 to 4 feet) shielded cable. However, it is per-

missible to use long cables to transmit the output signal of the General Radio Amplifier.

F. Filtering the Amplified Signal from the Crystal Pickup

As mentioned in the Introduction, the output signal of the pickup crystal is extremely complicated. One of the primary purposes of this investigation is to clean up this signal. Part of the task of cleaning up the signal can be accomplished by a better design of the test specimen. However, a large part of the cleaning up of the signal can be accomplished by filtering it in an appropriate manner. This will be explained more fully in Section IV. The extraneous 60 cycle pickup from the surroundings is also eliminated by filtering.

Two Spencer-Kennedy Variable Electronic Filters, Items E and F, were used. One filter, Item E, is shown in Figure 6. It is the top unit in the center rack.

Each filter consists of two units, each of which may be used either as a high pass or a low pass filter. Each unit in Item E has a range from 20 cps to 200 kc and each unit in Item F from 2 cps to 20 kc. These units can be ganged by putting two units, which have the same filter setting, in parallel. This produces a sharper filtering characteristic curve.

The reasons for placing the filters after the amplifier and before the oscilloscope are:

1) The filter units add a low level extraneous noise (between 60 and 100 microvolts per unit) to the signal passing through them. At the one volt signal level after the amplifier, this is insignificant. However, remembering that the ADP signal has a maximum amplitude of 1 to 2 millivolts, this noise could be significant if the filters would be placed before the amplifier.

2) The 60 cycle pickup should be removed just before introducing the signal into the oscilloscope. If the filter were located after the ADP crystal, some 60 cycle pickup could occur later in the circuit and never be eliminated.

G. Monitoring and Recording the Output Signal

The amplified and filtered signal output from the SKF filters is introduced into a Tektronix Oscilloscope, Item G. Records of oscilloscope traces are obtained using a Du Mont Oscillograph Recording Camera, Item H. The oscilloscope and camera are shown in Figure 6. The Type 53/54 D Plug-In Unit, Item G1, is used in the oscilloscope for all of the experiments involving ADP crystal pickups.

The oscilloscope sweep is triggered by the "Sync. Out"

from the Rutherford Pulse Generator. Except for small delays in the circuit, an oscilloscope sweep begins at each instant that a simulated acoustic emission, which is associated with the rise portion of the square electrical pulse, is initiated in the test specimen. The sweep rate is adjusted so that the sweep has completed before the signal associated with the fall portion of the square electrical pulse occurs (see part II C). A sweep occurs 5 times per second and, because of the retention of the screen, the signal appears to be constant on the scope. When the camera is used to record the signal, a "single sweep lock out" is used. This allows only one sweep to occur until it is reset.

II. Frequency Response of the ADP Crystals

In order to interpret the signal that is generated when the stress wave from a simulated acoustic emission excites the ADP crystal, it will be necessary to obtain a frequency response curve for each of the ADP crystals.

Sinusoidal stress waves having the same amplitude, but having different frequencies, do not produce the same amplitude output signals from the ADP crystal. It is expected from the theory of forced-damped vibrations (TI 55) that the exciting frequencies which are closest to the natural frequency of the crystal will produce the

largest output signals. The natural damping in the crystal prevents the output from diverging to infinity at the natural crystal frequency.

The frequency response curves are obtained experimentally. A uniform rod is used, rather than a shaped specimen, to eliminate the problems associated with the change of cross section.

If a semi-infinite rod were available, one could introduce a continuous sinusoidal stress wave at infinity and use an ADP crystal at the end to obtain the amplitude of the crystal output. In this case, reflections from the ends would not be a problem. The amplitude of the stress wave could be held constant while the frequency is varied. Then the amplitude of the ADP crystal output versus the frequency would provide the frequency response curve.

In the case of a finite rod, a continuous sinusoidal stress wave is reflected at both ends of the rod. Since the damping in the aluminum is not very large, there are a multiplicity of stress waves rattling around in the rod and no useful data can be obtained.

Therefore, for a finite rod, it is necessary to use a pulsed sinusoidal stress wave. The rod must be long enough to allow the direct pulsed wave to effect a complete crystal response at the crystal end before any

reflections from the other end arrive. It is necessary to use between 5 and 10 cycles in the pulse, to insure that steady state conditions are attained in the crystal output. This is easily determined experimentally.

The block diagram of the experimental setup used for these frequency response experiments is shown in Figure 10. A picture of the experimental setup is given in Figure 6.

A Pulsed Oscillator, Item J, was designed and constructed with the help of Mr. Albert Bowmell. It is shown in Figure 9 and can be seen in the foreground of Figure 6. The circuit diagram of the Pulsed Oscillator is given in Figure 11. It is capable of generating pulsed sinusoidal signals of approximately 100 volts having pulse widths up to about one millisecond with frequencies from 10 kc up to 200 kc.

A 130 inch long one inch diameter 2024 aluminum rod was used. A Barium Titanate input probe, placed so that the axis of the crystal is coincident with the axis of the rod (called "axial centerline position" hereafter), was located 37 inches from the ADP crystal end. As will be shown in part III C, the stress wave will be uniform across the cross section at a short distance from the input probe. The natural frequency of the Barium Titanate input crystal is about 1.7 megacycles. Since these

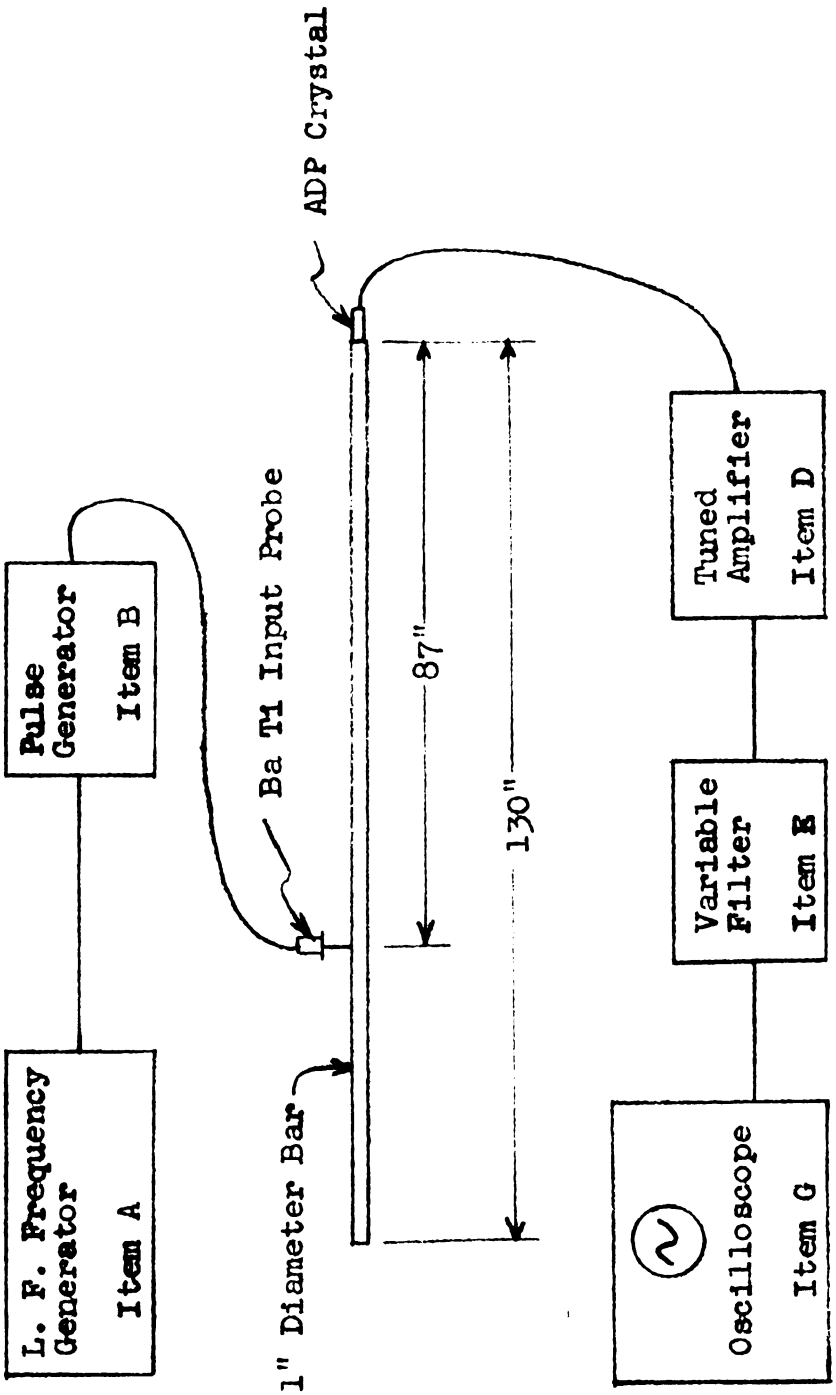

Figure 10. Block Diagram of Frequency Response Tests

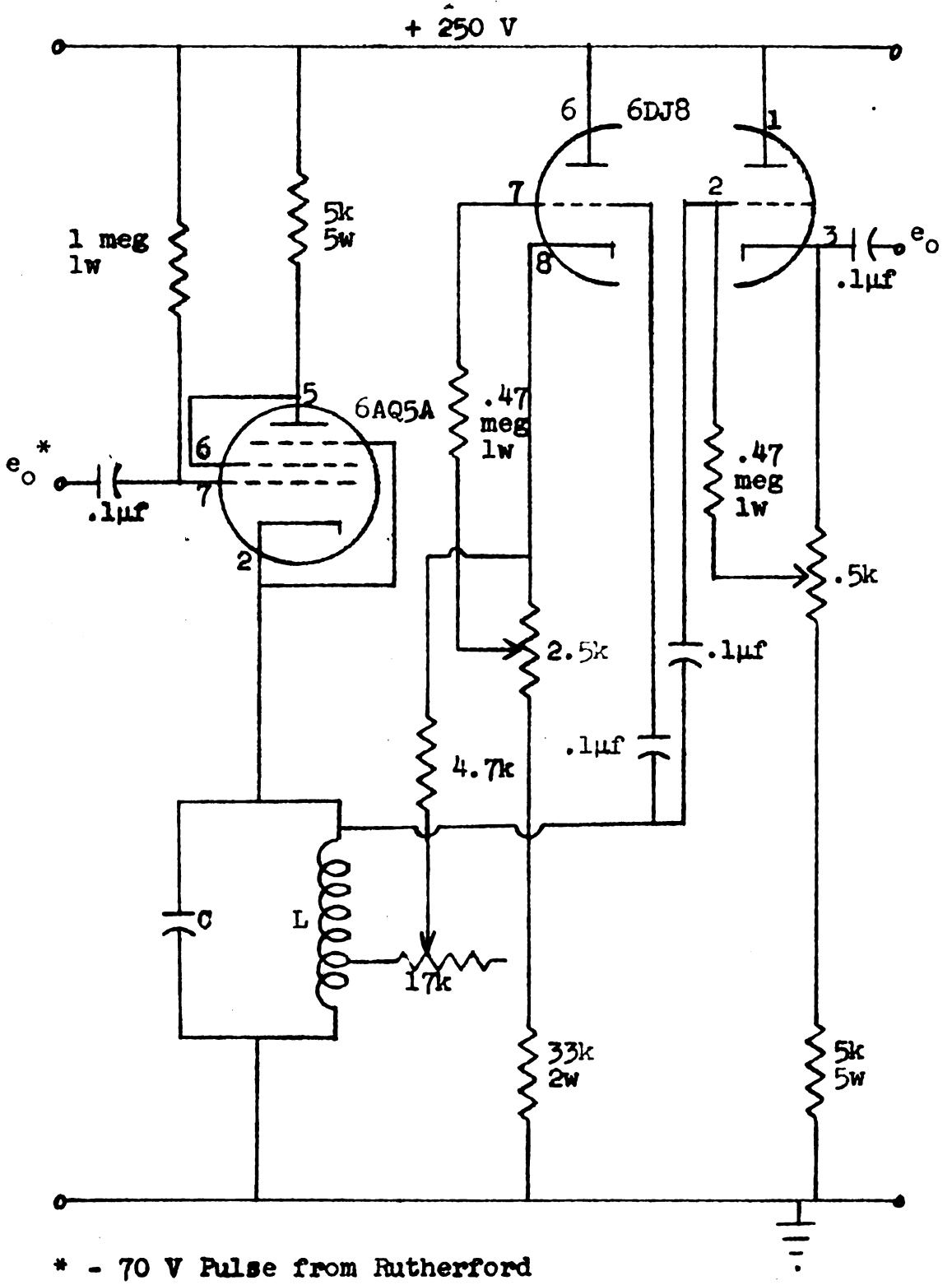

* - 70 V Pulse from Rutherford

Inductor is Stancor RTC-8624 12 to 35 mh.
The values of C vary from 150 µµf to 3900 µµf.

Figure 11. Circuit Diagram for the Pulsed Oscillator

frequency response tests do not exceed 130 kilocycles, it is assumed that there are no frequency response problems associated with the stress output of the Barium Titanate probe.

The test procedure is as follows:

1) The Rutherford Pulse Generator (Item B) triggered 5 times per second by the H.P. Function Generator (Item A), gates the Pulsed Oscillator with the selected pulse width (see Figure 6). The G. R. Pulse Amplifier (Item C) is not used.

2) The frequencies in the pulsed wave, generated by the Pulsed Oscillator, are determined by the L-C parallel part of the circuit (see Figure 11). The inductance is varied by adjusting the position of the iron core in the Stancor inductor. Different size capacitors may be plugged-in (see Figure 9). The output of the Pulsed Oscillator is displayed on an oscilloscope for purposes of adjusting its amplitude, pulse width and frequency. Then the Pulsed Oscillator output voltage is imposed on the input probe and a pulsed stress wave is originated in the rod.

3) The direct stress wave excites the ADP crystal, which is being tested, and the crystal output

is amplified and filtered. The SKL Filter, Item E, has one unit set on high pass and the other on low pass at the same frequency as the Pulsed Oscillator output. This eliminated any stray signals away from the test frequency.

4) The amplified and filtered signal is displayed on the oscilloscope, which has been triggered by the "Sync Out" from the Rutherford Pulse Generator. The sweep rate is adjusted so that only the direct pulse is displayed. The amplitude of the crystal output is obtained.

Both ADP crystals were tested in this manner at enough frequencies to allow plotting of the frequency response curves, which are given in Figure 12. The ordinate of these curves is the Relative Response, which is the millivolts of amplified crystal output (using the same amplifier gain) divided by the volts of the Pulsed Oscillator output, which was nearly a constant. The absolute value of the response is not important, because it depends on such parameters as the voltage applied to the input probe, the cross sectional area of the rod, the gain of the amplifier and the losses in the filter. These are all constants (a correction is made for the small variation in the voltage applied to the crystal) in this frequency response test. However, in later tests

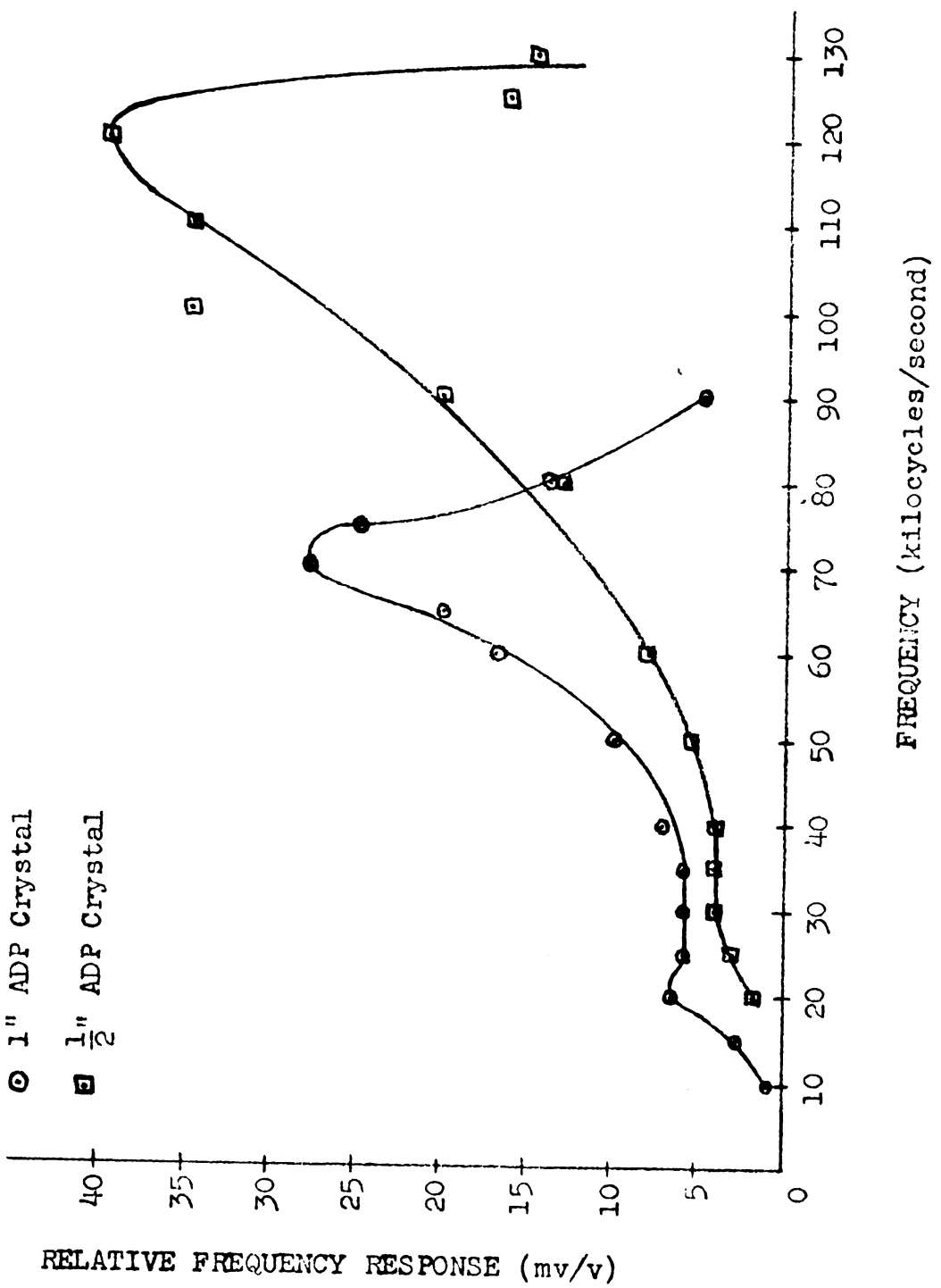

Figure 12. Frequency Response Curves

of the specimens, these parameters are not the same and only relative responses are significant.

In Figure 13, a typical oscilloscope record of the Pulsed Oscillator output and the corresponding amplified and filtered crystal response are shown.

A discrepancy may be seen in the response curve for the 1/2 inch ADP crystal at about 100 kc (see Figure 12). This can be attributed to a phenomenon known as "end resonance", which was first discovered experimentally by Oliver (OL 57). Later McNiven (MC 61) analytically proved the existence of the end resonance phenomenon. McNiven shows that there is a large amplification of the amplitude of the vibration at the end of the rod in a very narrow band of frequencies around the end resonance frequency, ω_R. McNiven shows that

$$\omega_R = .6767 \frac{3.8317}{a} \sqrt{\frac{\mu}{\rho}} = \frac{2.593}{a} \sqrt{\frac{\mu}{\rho}} \qquad \text{(II.1)}$$

For the one inch diameter aluminum rod used in this frequency response test ω_R = 102,300 cycles per second, which explains why the experimental value is too large at 100 kc. This end resonance frequency could have been raised above the 130 kc upper limit of these frequency response tests, if a rod of 3/4 inch diameter or less were used.

As mentioned in the Introduction, Schofield (LE 59) introduced stresses at one end of a specimen and detected them at the other end. He used identical piezoelectric crystals at each end of the specimen and used a pulsed oscillator to power the sending crystal.

Using this same method, an investigation was conducted by the author to determine if the "sensitive" frequency phenomenon found by Schofield exists for a uniform rod. No "sensitive" frequencies were found. Instead, the results of this investigation are similar to the curves of Figure 12. These would not be valid frequency response curves, because the sending ADP crystal obviously does not qualify as a frequency insensitive sender in the frequency range used.

The difficulty in Schofield's experiment seems to be the use of a relatively short shaped specimen. There are problems associated with the changing cross section and multiple reflections as will be explained more fully later. This explains the hash he found. The "sensitive" frequencies were probably due to an "in-phase" condition between the largest reflections. Schofield noted that these "sensitive" frequencies could not be correlated to the natural frequencies of the specimen.

III

ANALYTICAL PREDICTION OF THE MODES OF STRESS WAVE PROPAGATION

A. Discussion

Before proceeding with the experimental portion of this investigation, it is reasonable to attempt to predict the modes of stress wave propagation in the specimen. The analytical predictions will be made in this section. In Section IV experimental investigations, which verify the analytical predictions, will be reported.

As may be observed from Figures 1 and 3, each test specimen used in this investigation is a composite of many different components: cylinders, transition sections and large end sections (which are too short to be treated mathematically as cylinders). Separate components of these types are shown in Figure 4.

The mode of stress wave propagation in each separate component will be determined, using analytical methods from the existing literature, an extension of one method, and an original derivation. Then the components will be imagined to be joined to form the test specimen and a synthesis of the problem will be constructed. The resulting stress wave propagation in the entire specimen will be predicted.

There are numerous papers in the literature con-

cerning stress wave propagation in cylinders. These are the result of analytical and experimental research by the authors. Several of the more important papers are by Pochhammer (PO 76), Chree (CH 89), Bancroft (BA 41), Davies (DA 48), Mindlin and Herrmann (MH 51), Kolsky (KO 54), Tu and Brennen and Sauer (TU 55), Miklowitz (MI 56), Oliver (OL 57), Curtis (CU 60), Bell (BE 60), and McNiven (MC 56). Most of these papers are concerned with dispersion.

Dispersion is the following phenomenon. When a stress wave propagates along a cylinder, each Fourier component of the stress wave tends to travel at a different velocity. Dispersion causes a change of the shape of the stress wave with the distance traveled.

The effect of dispersion only becomes important for large travel distances of the stress waves. In a short specimen, these large travel distances can only be obtained after many reflections. It will be shown later that the changes in the stress wave resulting from the multiple reflections are far more important than the changes caused by dispersion.

However, the work of Bell (BE 60) mentioned above will be important in analyzing the stress wave propagation in the cylindrical test section. The works of Oliver (OL 57) and McNiven (MC 61) have already been used in part II H.

B. Mathematical Representation of the Acoustic Emission Source

Acoustic emissions are believed to be the result of the motion of dislocations. The source of an acoustic emission probably occupies a region which is small compared to the size of the test section.

The test specimens are made of 2024 aluminum rod, which is a polycrystalline material. It is possible for a large number of dislocation loops to be generated, perhaps by a Frank-Read source, within one of the crystallites of the polycrystalline material. These loops will pile up against the grain boundary and can later burst through the boundary, causing an acoustic emission. Therefore, the size of the region of the acoustic emission is roughly the size of the crystallite.

Ang and Williams (AW 59) have analytically determined the dynamic stress field due to an extensional dislocation moving at a constant velocity in an infinite medium. They have considered the problem as a two dimensional plane strain case. Their dislocation line is infinitely long and infinitely thin. The latter is a reasonable approximation, because Peierls (PE 40) and Nabarro (NA 47) have shown that the width of an edge dislocation does not exceed 7 or 8 atomic spaces. The infinite length approximation will be discussed later.

Ang and Williams have considered three velocity regimes: subsonic, transonic, and supersonic. However,

Eshelby (ES 49) has shown that the velocity of either an edge or screw dislocation cannot exceed the shear wave velocity, $v_s = \sqrt{\frac{\mu}{\rho}}$, which is the upper limit of the subsonic regime. In the subsonic regime, Ang and Williams have shown that two cylindrical waves are generated: 1) a dilatation wave having a velocity, $v_d = \sqrt{\frac{\lambda+2\mu}{\rho}}$ and 2) a shear wave having a velocity, $v_s = \sqrt{\frac{\mu}{\rho}}$.

A dislocation line in the specimen is confined to one crystal and is not infinitely long. In view of all of the forementioned considerations, it will be assumed that an acoustic emission creates a stress wave that is almost spherical. If the dislocation line were infinitely long, the stress wave would be cylindrical. However, the dislocation line is very short and the end effects would probably cause the stress wave to be cylindrical with hemispherical end caps. This can be idealized into a spherical stress wave.

The dislocation does not move at a uniform velocity. Instead, it accelerates very rapidly (about 10^{-9} second acceleration time) (CA 59), travels at a uniform subsonic velocity for a very short distance, and then decelerates rapidly. Therefore, instead of a continuous wave being generated, there will be an impulsive $\delta(t)$ type of wave generated. Here $\delta(t)$ is the Dirac Delta function, which is mathematically defined as $\delta(t) = \frac{1}{\varepsilon}$ for $-\frac{\varepsilon}{2} < t < \frac{\varepsilon}{2}$ as $\varepsilon \to 0$ and $\delta(t) = 0$ for all other t.

In summary: it will be assumed that an acoustic emission will create an impulsive $\delta(t)$ type of spherical dilatation wave and an impulsive $\delta(t)$ type of spherical shear wave, both having extremely short pulse widths. The dilatation wave travels with velocity, $v_d = \sqrt{\frac{\lambda+2\mu}{\rho}}$, and the shear wave with velocity, $v_s = \sqrt{\frac{\mu}{\rho}}$.

C. Stress Wave Propagation in the Test Section

The test section, taken as a separate component, is a cylinder of diameter, D_t, and length, T (see Figure 1). Somewhere in this cylinder the stress waves just described originate.

If these stress waves occurred in an unbounded medium, they would propagate as spheres of increasing radii. However, they occur in a bounded medium, the cylinder.

Consider first the dilatational wave. When this wave encounters the free surface of the cylinder, it must be reflected as two waves, one dilatational and one shear. The shear wave occurs because the surface of the cylinder is stress free and a dilatational wave alone cannot satisfy this condition. The two reflected waves would soon encounter another part of the cylindrical surface. Each would be reflected as two stress waves, one dilatational and one shear. In a very short distance, the one dilatational wave has multiplied into a great number of both dilatational and shear waves.

Bell (BE 60) has shown both analytically and experimentally that this large number of stress waves, instead of creating a hopelessly complicated stress wave, in fact create a stress wave which is uniform across the cross section and travels at the bar velocity, $v_b = \sqrt{\frac{E}{\rho}}$. He states that it requires about 3 to 5 bar diameters to accomplish this dynamic version of the St. Venant principle. An experimental investigation to determine the existence of a dynamic St. Venant principle has been made by Flynn and Frocht (FL 61).

Bell made several assumptions which should be noted here. 1) The source of the spherical dilatational stress wave is on the centerline of the cylinder, 2) The reflections at the free surface follow the same law as plane waves reflecting on a flat surface, and 3) the effect of the difference in curvature between dilatational and shear wave fronts is small in the time required for traversing a single diameter. The latter two assumptions are inherent to his analysis and are probably valid.

However, we will certainly have stress waves that do not originate on the centerline of the cylinder. By an extension of the dynamic St. Venant principle, at a sufficient distance from the source (probably 3 to 5 bar diameters), a uniform stress wave plus a small bending wave should exist. These small bending waves will probably be eliminated by the specimen support reactions before they reach the ADP crystal.

In a similar fashion, at 3 to 5 bar diameters from the source, the spherical shear wave from the acoustic emission source would become a uniform shear wave traveling at the shear wave velocity, $v_s = \sqrt{\frac{\mu}{\rho}}$. This stress wave is of no interest, because the ADP crystal, which is used to detect the stress waves at the end of the specimen, is sensitive to normal stresses only.

In summary: 1) For acoustic emissions which occur at least 5 bar diameters from the end of the test section, the pertinent stress wave is an impulsive $\delta(t)$ type of extensional wave, which is uniform across the cross section, traveling at the bar velocity, $v_b = \sqrt{\frac{E}{\rho}}$. 2) For acoustic emissions which occur at less than 3 to 5 bar diameters from the end of the test section, the stress wave is close to uniform across the cross section and will probably be averaged out in its travel through the transition section. In any event, if the test section is at least 10 diameters long, then the stress wave traveling in the opposite direction will become uniform. If there is an ADP crystal at each end of the test specimen, the acoustic emission will be detected accurately at least at one end.

D. Stress Wave Propagation in the Transition Sections

The transition sections, taken as separate components, are bell-shaped axiallysymmetric pieces, tapering from

diameter, D_t, up to diameter, D_m, in a longitudinal distance, F. The radius of curvature of the generatrix is R (see Figure 1). A separate transition section component for the large size specimens is shown second from the left in Figure 4.

An impulsive $\delta(t)$ type of extensional stress wave, which is traveling at a velocity, v_b, will be introduced from the test section into the small end of the transition section. Its propagation through the transition section is determined in Appendix A.

Several assumptions have been made in Appendix A concerning the stress wave propagation through the transition section.

1) The stress wave is purely extensional and is uniform across the cross section.
2) The stress wave propagation in the actual transition section does not essentially differ from the propagation through a transition section which has the shape of an exponential horn. See Appendix A for the details of this assumption.

It is shown in Appendix A that the impulsive $\delta(t)$ type of extensional stress wave travels through the transition section at velocity, v_b. It is uniform across the cross section and the amplitude of both the stress and strain vary as the inverse ratio of the diameters.

In summary: An impulsive $\delta(t)$ type of extensional

stress wave travels through the transition section at velocity, v_b. The amplitude of the stress wave varies as the inverse ratio of the diameters. Therefore, the amplitude of the stress wave at the large end of the transition section is 1/2.5 = 0.4 as large as its amplitude at the small end of the transition section.

E. Stress Wave Propagation in Cylindrical Outer Sections

All but two of the test specimens, used in these experiments, contain cylindrical sections of length, M, and diameter, D_m, between the transition sections and the end sections (see Figure 1).

An impulsive $\delta(t)$ type of extensional stress wave, which is uniform across the cross section, will be introduced from the transition section into this cylindrical section. It will propagate through the cylinder at the bar velocity, v_b. Any possible dispersion effects will be very small and, as will be shown later, are negligible compared to the effect of the reflections.

F. Stress Wave Propagation in the End Sections

The end sections, taken as separate components, are short cylinders of diameter, D_e, and length, L_e (see Figure 1).

An impulsive $\delta(t)$ type of extensional stress wave, which is uniform over a circular area of diameter, D_m, is

introduced at surface B of the end section. This stress wave comes from the cylindrical outer section or, for the test specimen without these sections, from the transition section. Notice that the stress wave acts over only one fourth of the total area of surface B. Since the end section is very short and the stresses at the surface B are not uniform across the entire cross section, the end section cannot be analyzed as a cylinder.

The end section will be analyzed by considering it to be a half-space with a uniform amplitude $\delta(t)$ type of impulsive load over a circular area on the surface and with the remainder of the surface stress free. The surface of the half-space is surface B of the test specimen (see Figure 1). After the stress wave propagation in the half-space is determined, the effect of reflections from the curved cylindrical side and the end (surface A) of the end section will be considered.

The analysis of the half-space with the $\delta(t)$ impulsive load is given in Appendix B. The results of the analysis are (see Figure B1 in Appendix B):

1) The main stress wave propagation consists of a $\delta(t)$ type of impulsive extensional stress wave, having the same diameter as the load, traveling into the half-space with a velocity, v_d. For brevity, this will be called the "$\delta(t)$ head".

2) There also exist $\delta(t)$ type of impulsive spherical wave fronts, which have small amplitude compared to the "$\delta(t)$ head", traveling with a velocity, v_d.

Now consider that the end section is not a half-space, but is bounded by the curved cylindrical surface and the end (surface A).

The spherical dilatation impulsive waves will strike the curve side and be reflected as both dilatational and shear waves. But their amplitude is small and the effect of these reflected waves will be correspondingly small.

The "$\delta(t)$ head" will not encounter the curved side. It will, however, encounter the end (surface A) of the end section. It will be reflected back into the end section with a change in sign, just as any extensional stress wave which has normal incidence on a free surface. The "$\delta(t)$ head" only sweeps out about one fourth of the cross sectional area of the end section. Thus, there is sufficient material, which is practically unstressed, surrounding the path of the "$\delta(t)$ head" to make the half-space analysis valid.

G. Stress Wave Propagation in the Entire Specimen

The stress wave propagation in each of the separate components of the specimen was determined in parts III C through III F. In this part, the components will be

imagined to be joined together and the stress wave propagation in the entire specimen will be predicted.

For convenience, the specimen geometry, without dimensions, is given in Figure 14 below.

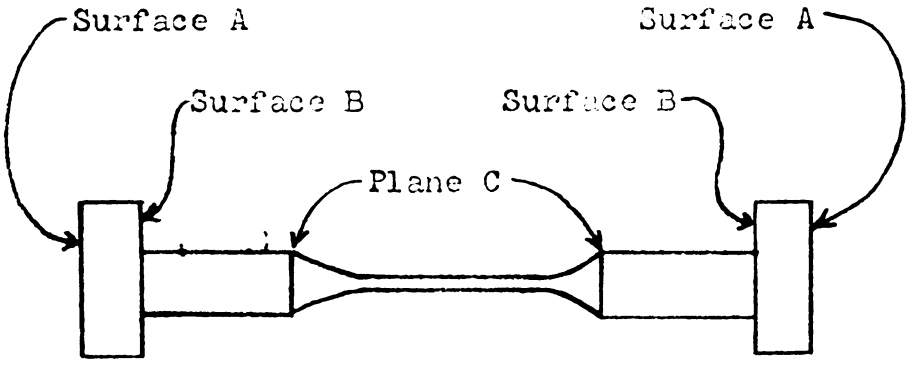

Figure 14. Specimen Geometry

The following stress wave propagations should be produced as the result of the occurrence of an isolated acoustic emission in the test section.

1) Two uniform $\delta(t)$ type of impulsive extensional stress waves, one traveling toward each end of the specimen, will be developed in the test section at about 3 to 5 diameters from the acoustic emission source. These waves travel at the bar velocity, v_b.
2) Each wave travels through its respective transition section at the bar velocity, v_b. The amplitude of the wave varies inversely as the

diameter ratio. Therefore, at plane C, the amplitude is 40% as large as when it entered the transition section.

3) At plane C, there could be a reflection, because of the discontinuity in the rate of change of area with longitudinal distance. However, since there is no discontinuity in area, this reflection would be extremely weak and is considered to be negligible.

4) If a cylindrical section between the transition section and the end section exists, then the stress wave at plane C travels through this section at the bar velocity, v_b, and with no change of amplitude or shape. This neglects dispersion.

5) At surface B, the uniform extensional stress wave, which comes from the outer cylindrical section or the transition section (depending on the particular specimen geometry), is partly transmitted into the end section and partly reflected back into the outer cylindrical section (or transition section).

Ripperger and Abramson (RI 57) used an approach based on elementary theory to find the reflection and transmission of elastic pulses at a discontinuity in cross section. They conducted

experiments and found fair correlation with the theory. However, at the present time, this is the best theory available. Their results for the case of a discontinuity in cross section only, with no change of material or material properties across the discontinuity, are

$$\sigma_r = \frac{A_2 - A_1}{A_1 + A_2} \sigma_i \qquad \text{(III.1)}$$

$$\sigma_t = \frac{2A_1}{A_1 + A_2} \sigma_i \qquad \text{(III.2)}$$

where σ_i, σ_r, and σ_t are the amplitudes of the incident, reflected and transmitted waves respectively, and A_1, A_2 are the areas upstream and downstream of the discontinuity respectively.

It should be noted that Ripperger and Abramson considered a discontinuity in cross section between two long cylinders. They assumed that the stress was uniform across the entire cross section on both sides of the discontinuity. For long cylinders, this will be inexact only for about 3 to 5 bar diameters from the discontinuity in the larger cylinder. This is, again, the dynamic St. Venant principle.

However, for the discontinuity at surface B of the specimen, this is a very poor assumption. As was seen in part III F, the stresses in the end section are not uniform across the cross section. Instead, only one fourth of the cross section is stressed by the"δ(t) head", and the rest is relatively stress free. Therefore, equations (III.1) and (III.2) can only be used as rough estimates.

Physical reasoning can be used to show that stress waves will be reflected and transmitted at surface B of the specimen. If the end section had an infinite mass, then surface B would be fixed and the entire incident wave would be reflected with no change in sign. But the mass of the end section is finite, and a large percentage of the wave is reflected with no change in sign. The remainder of the wave is transmitted into the end section with no change in sign. This creates the "δ(t) head" in the end section and accounts for the motion of the center of gravity of the end section due to the impulse imparted to the end section.

According to the Ripperger approximation, 60% of the wave at surface B is reflected back into the specimen, and 40% is transmitted into

the end section, because $A_2 = 4A_1$ in equations (III.1) and (III.2). There is no change in sign for either wave.

6) Only approximately (.4)(.4) = .16 or 16% of the amplitude of the original test section stress wave, which was traveling toward one of the end sections, enters that end section. This creates the "δ(t) head", which travels from surface B to surface A at the dilatational velocity, v_d. It is reflected at surface A with a change of sign, but no change of shape or amplitude. An ADP crystal on surface A will detect this wave. This is the first effect of the acoustic emission that is sensed by the ADP crystal.

7) The "δ(t) head" with a change of sign travels from surface A to surface B. At surface B, it will probably enter the outer cylindrical section with only a change of velocity from v_d to v_b. The diameter of the "δ(t) head" is identical to the diameter of the outer cylindrical section and no reflections are necessary to change its amplitude. The change in velocity is due to the different boundary conditions at the outer diameter of the "δ(t) head". In the end section, the boundary is essentially fixed

and in the outer cylindrical section, it is free.

8) Notice that two reflected waves are now traveling back down the specimen: one reflected from surface B with the same sign as the incident wave, and the other reflected from surface A with a change in sign from the incident wave. The former wave has approximately 1.5 times the amplitude of the latter. Each waves travels at the bar velocity, v_b. The former wave leads the latter by $\frac{2L_c}{v_d}$ seconds.

9) When these two reflected waves each reach plane C, they could enter the transition section with no reflections taking place. This was assumed for the wave traveling in the opposite direction at plane C (see 3). However, when a wave at plane C enters the transition section, it encounters a rapid decrease of cross section. Intuition would cause one to suspect that some of the wave would be reflected with a change of sign. Most of the wave would be transmitted with no change of sign. The fact that this reflection does exist will be shown experimentally in part IV H.

10) The two reflected waves from plane C will travel back toward the ADP crystal at surface A. Part will reach surface A and part will be reflected

at surface B.

11) The two reflected waves from surfaces B and A at the other end of the specimen will travel back toward the ADP crystal on surface A. Part will be reflected at plane C (nearest the other end), part will be reflected at surface B and part will reach the ADP crystal at surface A.

In summary: There will be a series of $\delta(t)$ type of impulsive extensional stress waves arriving at an ADP crystal on one of the surface A ends of the specimen. The first is the direct wave from the acoustic emission. This is followed by many waves of both signs that have been reflected from the various surfaces and planes of the specimen. These later waves are smaller than the direct wave, not because of the damping of the aluminum nor because of dispersion effects, but because their amplitude is reduced at each reflection.

H. An Optimum Specimen Design Based on the Theory

As just described in part G, many impulsive stress waves reach the ADP crystal at surface A. The direct stress wave is the significant one, and all the others tend to "hash" the signal.

The reflections of the waves occur at surfaces A and B and planes C. Surface A is obviously indispensable.

Surface B is used to apply the load to the specimen from the testing machine. If the ratio of the area of the end section to the area of the outer cylindrical section could be reduced, then the amplitude of the direct wave would be greater, because less of the direct wave would be reflected at surface B. However, this ratio is about as small as practical already.

But if surface B and plane C were made identical by eliminating the cylindrical outer section, then plane C is brought very close to the surface A. Thus, the reflected wave from surface B will not be partially reflected back from plane C toward the ADP crystal as before. Also, the reflected wave from surface A reaches plane C much sooner and is partially reflected back toward the ADP crystal. This reflected wave arrives at the ADP crystal very soon after the direct pulse $(\frac{2L_c}{v_d})$. Both waves have the same sign and tend to increase the ADP crystal output.

The variations between specimen geometries L1, L2, and L3 are used in part IV K to verify this hypothesis of a better specimen design.

This is about all the optimization that can be accomplished by good specimen design. The remainder of the optimization must be accomplished in the electronic instrumentation and also by the method described next.

I. Theory of Steel End Caps for the Specimen

During the experimental work, it was discovered that a steel plate placed on surface A between the ADP crystal and the specimen eliminated much of the "hash" from the signal. The theory of the effect of the steel plate on the stress wave propagation in the specimen will be given here.

The steel plate has the same diameter, D_e, as the end section, and its thickness is t_s. The steel plate is held in place on surface A of the specimen by a thin layer of the High Vacuum Grease mentioned in part II B. The ADP crystal is held in place on the steel plate by the High Vacuum Grease, just as it would be on surface A of the specimen if no steel plate were used. The steel plates may be seen clearly in Figure 3.

A stress wave which arrives at surface A from inside the specimen encounters a sudden change of acoustic impendance, ρv, between the aluminum and the steel.

Lindsay (LI 60) gives the solution for the wave propagation across a boundary. He considers the boundary to be the division between two half-spaces having different acoustic impendances. The stress wave is traveling normal to the boundary. He finds

$$\sigma_r = \frac{\frac{\rho_2 v_2}{\rho_1 v_1} - 1}{1 + \frac{\rho_2 v_2}{\rho_1 v_1}} \sigma_i \qquad \text{(III.3)}$$

$$\sigma_t = \frac{2}{1 + \frac{\rho_2 V_2}{\rho_1 V_1}} \sigma_i \qquad \text{(III.4)}$$

where σ_i, σ_r and σ_t are the amplitude of the incident, reflected and transmitted stress waves respectively, and the subscript "1" refers to upstream quantities and "2" refers to downstream quantities.

The velocity in steel and aluminum are practically identical, so equations (III.3) and (III.4) become

$$\sigma_r = \frac{\frac{\rho_2}{\rho_1} - 1}{1 + \frac{\rho_2}{\rho_1}} \sigma_i \qquad \text{(III.5)}$$

$$\sigma_t = \frac{2}{1 + \frac{\rho_2}{\rho_1}} \sigma_i \qquad \text{(III.6)}$$

The density of the steel is approximately three times the density of aluminum. Therefore, $\frac{\rho_2}{\rho_1} = 3$ and $1/3$ for the stress waves traveling from the aluminum into the steel and from the steel into the aluminum respectively. When these are substituted into equations (III.5) and (III.6),

1) For a stress wave traveling from the aluminum into the steel

$$\frac{\sigma_r}{\sigma_i} = \frac{1}{2} \quad \text{and} \quad \frac{\sigma_t}{\sigma_i} = \frac{1}{2} \tag{III.7}$$

2) For a stress wave traveling from the steel into the aluminum

$$\frac{\sigma_r}{\sigma_i} = -\frac{1}{2} \quad \text{and} \quad \frac{\sigma_t}{\sigma_i} = \frac{3}{2} \tag{III.8}$$

The aluminum end section of the specimen satisfies the half-space condition of Lindsay's solution. However, the steel plate is thin and certainly is not a half-space. It will be assumed here, that the stress waves enter the steel and traverse the thickness, t_s, as given by Lindsay. When they encounter the free surface of the steel plate, they will be reflected with a change of sign, just as any extensional stress wave which has normal incidence on a free surface.

When a single extensional wave, which is traveling in the end section of the specimen toward surface A, strikes the aluminum steel interface, part of the wave is reflected back into the end section and part is transmitted into the steel. The transmitted wave is reflected at the free surface of the steel with a change of sign and travels back to the steel-aluminum interface. There it is partly transmitted into the end section and partly reflected

back into the steel with a change of sign. Therefore, there are multiple reflections inside the steel plate with a gradual transmission of the wave into the end section.

The stress wave propagation caused by an isolated extensional wave striking the aluminum-steel interface is shown in Figure 15. The arrows show the direction of stress wave propagation and the plus and minus signs show tension and compression respectively. For convenience, the incident wave is taken to be a unit amplitude tensile wave.

Time increases down the columns. Take zero time to be when the unit incident wave strikes the aluminum-steel interface. The first wave that excites the ADP crystal arrives at time, $\frac{t_s}{v_d}$. Then a new wave arrives at the ADP crystal every $\frac{2t_s}{v_d}$ seconds. At t = 0, the first wave is reflected back into the specimen. Then a new wave enters the specimen from the steel every $\frac{2t_s}{v_d}$ seconds. The time intervals $\frac{2t_s}{v_d}$ are of the order of 2 microseconds, because the steel plate is 3/16 inch thick.

Now consider the difference between 1) mounting the ADP crystal on surface A of the specimen and 2) using a steel plate between surface A and the ADP crystal. For both cases, a unit tensile incident wave is assumed. In Figure 16, the stress waves that excite the ADP crystal

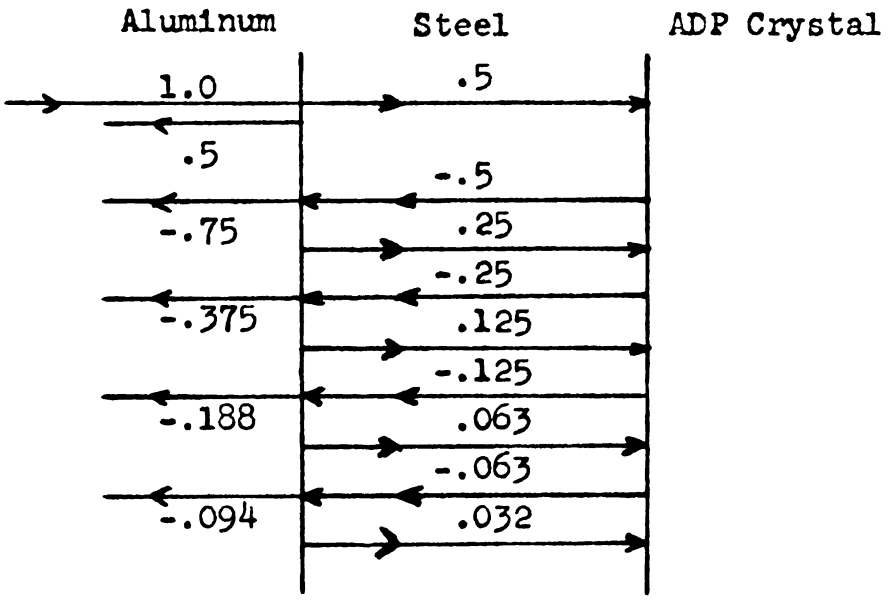

Figure 15. Stress Waves Associated with a Steel End Cap

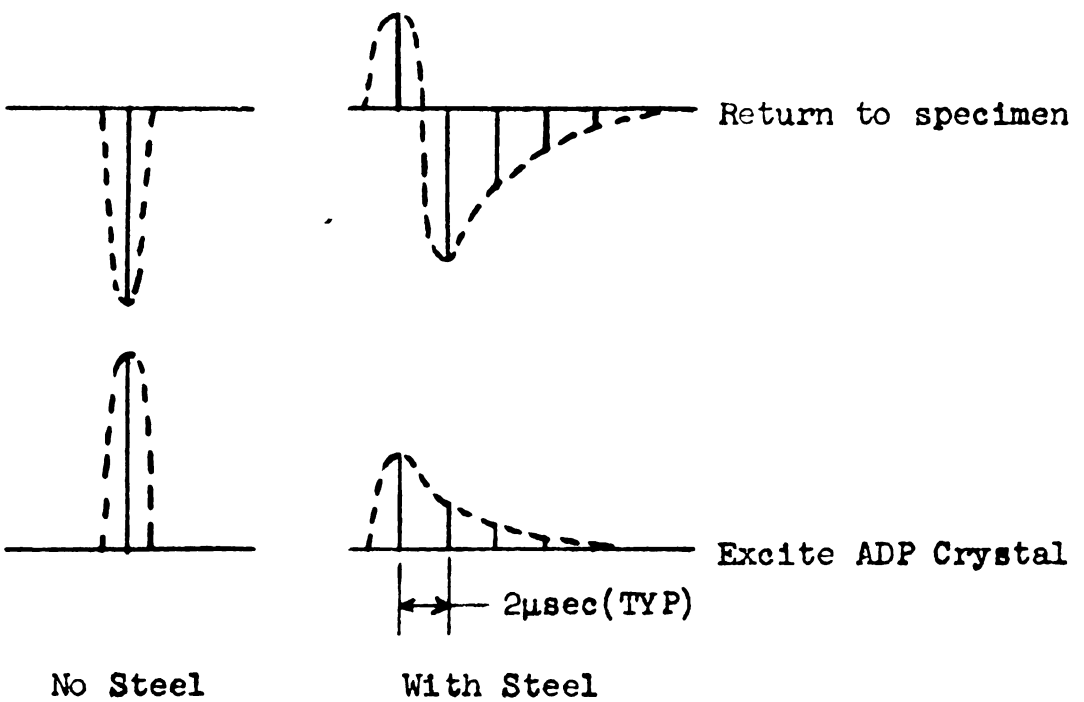

Figure 16. Comparison of Stress Waves that Excite the ADP Crystal and Return to the Specimens with and without Steel End Cap

and the stress waves that are returned into the specimen are shown for both cases. When the steel plate is used, the ADP crystal effectively feels a lower amplitude and larger pulse width stress wave. The ADP crystal will respond with a smaller signal. The stress wave which returns to the specimen has less amplitude, and has a larger pulse width. This stress wave also has a positive and negative peak of nearly equal amplitudes that occur within 2 microseconds. Because of the inertia of the ADP crystal, these would tend to cancel.

The reduced ADP crystal output is a disadvantage and the altered reflection is an advantage.

This analysis has the implicit assumption that the boundary between the aluminum and steel is perfect. Actually, High Vacuum Grease is used in this boundary and there will certainly be some losses in the grease. As will be shown in part IV D, a thin layer of grease is rather efficient, but a thicker layer has large losses.

IV

EXPERIMENTAL VERIFICATION OF THE MODES OF STRESS WAVE PROPAGATION

A.. Discussion

In part III G, the modes of stress wave propagation through the separate components of the specimen and through the entire specimen were predicted.

In this section, a series of experiments will be conducted to verify these predictions. In addition to establishing the validity of the theory, these experiments are concerned with the effect of specimen geometry on the stress propagation and on the signal which is read on the oscilloscope.

Additional experiments will be conducted to determine how varying the electronic instrumentation and using steel end caps affect the signal, which is read on the oscilloscope.

The ultimate purpose of all of these experiments is to determine an optimum system design, consisting of specimen, instrumentation, and experimental technique for the study of acoustic emissions. This amounts to obtaining a relatively "clean" signal on the oscilloscope for the occurrence of each acoustic emission. Therefore, in this entire section, the emphasis will be placed on "cleaning up" the signal on the oscilloscope. An example of the

signal before any "hash" has been removed is shown in Figure 17. However, all of the extraneous signals, which will be described in part IV C, have been removed.

B. Response of an ADP Crystal to a $\delta(t)$ Impulsive Stress Wave

In part III G, it was predicted that the ADP crystal would be excited by a series of $\delta(t)$ type of impulsive extensional stress waves. It is necessary to determine the ADP crystal output that results from the isolated incidence of one of these stress waves at the crystal.

An analytical solution of this problem has not been attempted. It would involve solving the problem of the vibration of a continuous prismatic elastic bar, which is free on one end and fixed on the other, having a prescribed $\delta(t)$ type of displacement initially at the fixed end. This would be a transient vibration, because of the natural damping of the crystal. Once the vibration were found, the voltage output of the crystal would have to be determined.

However, the formulation of the analytical problem can be used to explain why the use of a clamp and steel pressure block to fasten the crystal onto the specimen creates problems. This difficulty was mentioned in part II D. The clamp and block change the boundary conditions of the problem. Therefore, the entire response would be changed. The amount of pressure from the clamp

and the mass of the block could vary from test to test and cause serious complications.

The ADP crystal output, resulting from a $\delta(t)$ stress wave, was determined experimentally as follows:

1) A 1" long ADP crystal was mounted on the bottom end of a 30" long 1" diameter steel bar, whose axis was vertical.
2) A 2" long 1/2" diameter hardened steel bar, with a slightly rounded nose, was dropped on the top end of the 1" bar from a height of 6 feet.
3) The resulting stress pulse was monitored by 2 strain gages, which were placed 180° apart at 10" from the top of the bar, and arranged in a Wheatstone bridge, so that bending was eliminated and pure axial strain was sensed. The output was displayed on the Tektronix oscilloscope with a type E plug-in unit (Item G2), which was externally triggered by a pulse from a 1" long, 1" diameter Barium Titanate crystal, mounted on the side of the bar 5" above the strain gages.
4) When the stress pulse reached the bottom end of the bar, it excited the ADP crystal. The resulting crystal output was attenuated by a factor of 100, filtered using Item E, and displayed on another Tektronix scope. This

scope was externally triggered, using the "gate delay" from the first scope. The "gate delay" was adjusted to trigger the sweep just before the ADP signal began. Both oscilloscopes had completed their sweep before any reflections were sensed by the gages or the ADP crystal.

The experimental results are shown in Figure 18.

The stress pulse is shown in Figure 18a). It is a $\delta(t)$ stress wave having roughly 60 microseconds pulse width. It is difficult to obtain a shorter pulse by this method, because a 2" long drop bar represents a practical minimum. However, the ADP crystal output obtained here, should be indicative of its response to the shorter and lower amplitude stress pulse from an acoustic emission.

The unfiltered ADP crystal response is shown in Figure 18b). It consists of a fast rise time portion followed by a "ringing down" portion, which begins at the peak of the fast rise time portion.

After the crystal output has reached its peak, it should return to zero output rapidly. However, the crystal is excited by the impact and it vibrates for a short time at its natural frequency. This is demonstrated by Figures 18c) and d). Figure 18c) is the unfiltered signal of b) with the natural frequency component filtered off. It is similar to the $\delta(t)$ stress pulse that excites the ADP crystal. Figure 18d) shows the natural frequency

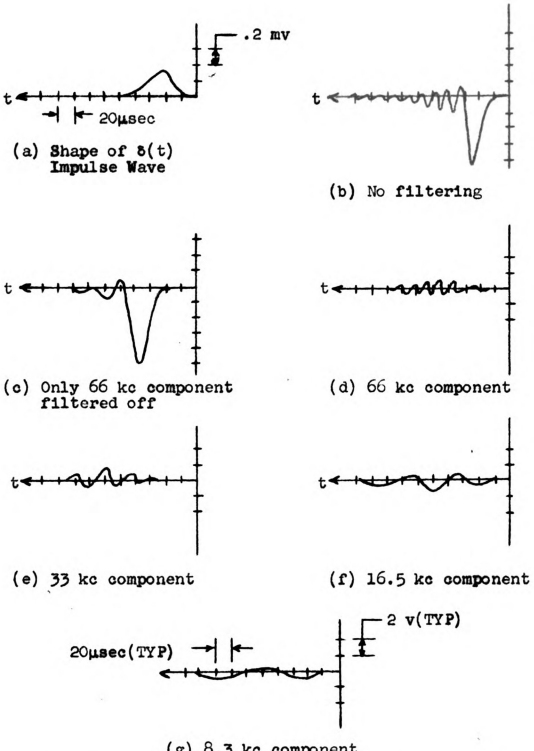

Figure 18. Response of ADP Crystal to δ(t) Impulsive Stress Wave

component alone. It is obviously a damped free vibration resulting from the initial disturbance of the crystal by the stress pulse. This demonstrates that the ADP crystal output consists of two parts

1) A $\delta(t)$ response, which is similar to the excitation.
2) A damped free vibration at the natural frequency.

It may be further shown that the part of the $\delta(t)$ response (part 1 above) which follows the peak consists of components having the subharmonic frequencies of the crystal. The first three subharmonic frequencies are shown in Figure 13e) through g) respectively. Notice that the amplitude of each component decreases, that is first subharmonic > second > third, etc. Also, notice that each component begins at the time the $\delta(t)$ response has reached its peak.

The damped free vibration part of the ADP crystal output (part 2 above) would be expected to have components at the natural frequency and all of the harmonic and subharmonic frequencies. However, it may be seen from the frequency response curves of Figure 12, that the natural frequency component will be the dominant one. The first subharmonic component is the next largest. The natural frequency component is 4.6 times as large as the first subharmonic component. For this reason, the damped free

vibration of part 2) above is considered to consist of only the natural frequency component.

In this experiment, the amplitude of the damped free vibration at the natural frequency and the first subharmonic component of the $\delta(t)$ response were nearly equal. This is not always the case. An experiment which almost duplicates this one was performed. Instead of dropping a small bar on the 1" diameter bar, a BB was fired against the top end of the bar. The resulting stress pulse had about 15 microseconds pulse width, but it was followed by a low amplitude "tail" of oscillations. This is a shorter pulse and the oscillations in the tail did not seriously affect the experimental results. In this case, the damped free vibration at the natural frequency had about twice the amplitude of the first subharmonic component of the $\delta(t)$ response. This, plus the general experience gained in monitoring the crystal response due to the simulated acoustic emissions (which have even shorter pulse width), leads to the conclusion that the ratio of the damped free vibration at the natural frequency to the first subharmonic component of the $\delta(t)$ response increases as the stress pulse width increases.

The 1/2" ADP crystal was also tested, using the 2" drop bar, and the same conclusions were reached.

C. Effect of Filtering

One of the main purposes of the filters, is to remove

60 cycle pickup. It was also found that the specimens vibrated at their spring-mass frequency, which was about 2 kc. This is a persistent vibration and is not easily identified with the number of acoustic emissions which occur in the specimen. Therefore, the filters are used to remove this component. High frequency signals from a short wave station were also eliminated by filtering. All of these filtering operations can be classified as rejection of unwanted extraneous signals, which are not directly associated with the acoustic emission.

However, the filters serve another equally important function. Even if all of the extraneous signals have been eliminated, the ADP crystal will give a relatively complicated output as shown in Figure 18b). The filters may be used to reject certain components of this output, such as the natural frequency. Or they may be used to retain only one component of the output, such as the natural frequency or the first subharmonic.

Several of these schemes of filtering have been used in the experimental investigations. The two found to be most useful are

1) Retaining only the first subharmonic frequency.

2) Reject only the natural frequency.

D. Effect of the Condition of the Grease Seal

The ADP crystal is mounted on surface A of the

specimen or on the face of the steel end cap, using High Vacuum Grease.

It is important to insure that the grease consists of a uniform thin film. If the grease is not uniform, it is obvious that some parts of the seal will be faulty and the effective area of the seal will be reduced. However, a thick layer of grease, even if it is uniform, will not serve as a reliable seal. Part of the signal will be lost in the grease. This is shown experimentally in Figure 19.

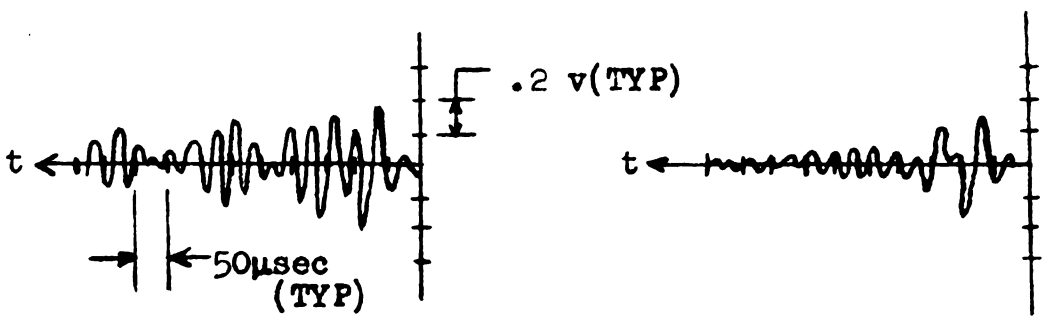

(a) Uniform Thin Seal (b) Uniform Thick Seal

Figure 19. Effect of the Grease Seal

Figure 19 a) shows the ADP signal at surface A of a test specimen having a uniform thin grease seal. Figure 19 b) shows the ADP signal under the same conditions, except a relatively thick grease seal is used. Notice that some of the amplitude of the signal is lost. Also, much of the detail of the signal is completely lost.

The steel end cap is mounted on surface A of the specimen with the same High Vacuum Grease. The stress wave propagation across the aluminum-steel boundary must be the same as if they were fused together. Only a thin layer of grease will approach this condition.

E. Effect of the Steel End Caps

The theory for the steel end caps was given in part III I. Their main advantage was that they changed the shape of the reflected wave at the end of the specimen from a $\delta(t)$ stress wave to a wave having the shape in Figure 16. This wave has a lower amplitude and tends to cancel itself out by an initial rapid change of sign. This reflected wave is expected to excite less ADP crystal response than the $\delta(t)$ reflected wave.

This is verified by the following experiment:

1) A 130" long 1" diameter aluminum bar has a Barium Titanate input probe located in the "axial centerline position" at 45" from the 1" ADP crystal end.
2) A $\delta(t)$ type impulsive stress wave was introduced into the bar in the same manner as described in part II C.
3) The ADP output signal was filtered so that only the first subharmonic component was passed.
4) The sweep rate of the oscilloscope was adjusted

to allow viewing of the ADP crystal response caused by the direct stress wave and the first two reflected stress waves.

This experimental setup is similar to that shown in Figure 8 (the pulsed oscillator in the foreground was not used).

The results are shown in Figure 20. In Figure 20 a), the second and third signals are reflections. In Figure 20 b), both of these reflected signals are essentially eliminated by placing a steel plate at the end of the bar opposite the ADP crystal. This steel plate may be seen at the far end of the bar in Figure 8. This shows that the reflected signal from the end of a bar having a steel cap is changed in such a manner that it cannot excite an appreciable response in an ADP crystal.

It was observed in many of the experiments, that the amplitude of the direct stress wave was cut approximately in half when a steel plate was used at the ADP crystal end. This agrees with the theory of part III I.

F. Dynamic St. Venant Principle Used in Test Section

The acoustic emission acts as a point source at some point in the test section. In part III C, it was predicted that the stresses become a $\delta(t)$ type of extensional stress wave, which is uniform across the cross section,

within 3 to 5 bar diameters of the source.

This was confirmed experimentally as follows. The experimental setup is identical to that used in part III E above, except that the distance from the Barium Titanate input probe to the ADP crystal end was changed from 87" to 43" to 20" to 10" to 5".

The results show that ADP crystal output caused by the direct pulse was essentially the same in all cases. Thus, as long as the acoustic emission occurs at least 5 bar diameters from the end of the test section, the resulting stress wave will be uniform across the cross section.

In part III B, it was assumed that the stress wave originating at the acoustic emission source could be idealized as spherical, although it is probably cylindrical with hemispherical end caps. Also, in part III C, it was assumed that the stress wave resulting from an acoustic emission which is not located on the centerline of the specimen would not be different than that resulting from one on the centerline.

The validity of both of these assumptions can be proved as follows. The simulated acoustic emission from the Barium Titanate input probe certainly is directional and not spherical. This simulates the non-spherical character of the actual acoustic emission. Experiments

were performed which were identical to those used to verify the dynamic St. Venant principle, except that the input probe was also moved radially and turned as much as 90°. In each case, the results show that the ADP crystal output caused by the direct pulse was essentially the same shape, but not of the same amplitude.

G. Stress Waves in the Transition Section

In part III D, it was predicted that the $\delta(t)$ impulsive stress wave travels through the transition section at the bar velocity, v_b. Its amplitude varies as the inverse ratio of the diameters.

An experiment was performed that verified this behavior in the transition section, in addition to some other stress wave propagation properties. The details of the experiment and the experimental results are given in part IV J below.

H. Stress Wave Propagation in the Cylindrical Outer Section

In part III E, it was predicted that the $\delta(t)$ impulsive stress wave travels through the cylindrical outer section at the bar velocity, v_b. Neglecting dispersion, there is no change in the stress wave. It was also predicted in item 9) of part III G that a stress wave, which

was traveling in this section toward the transition section, would be partly reflected when it reached plane C.

Both of these predictions were verified by the following experiment. Essentially the same experimental setup, as described in part IV E above, was used. However, in this experiment the second component from the right in Figure 4 was mechanically positioned on the end of the 1" diameter bar. High Vacuum Grease was used in the joint. A 10" long 2-1/2" diameter aluminum bar was mechanically positioned on the end of the shaped component, using High Vacuum Grease. See Figure 21 for a sketch of the specimen geometry. Figure 22 shows

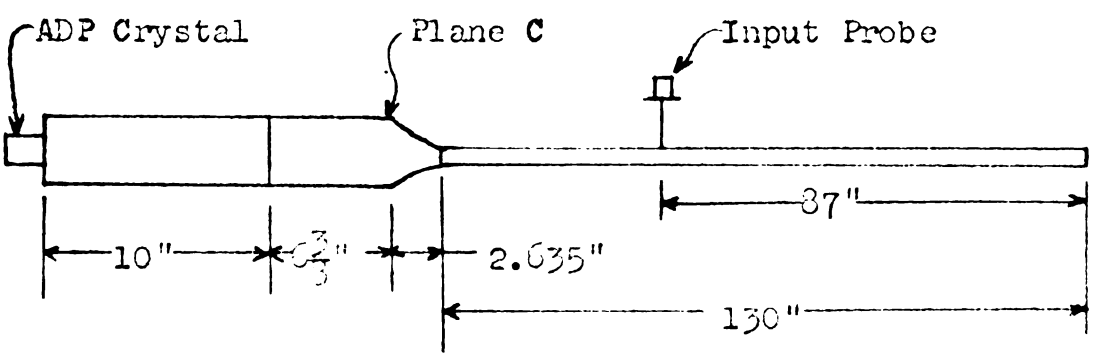

Figure 21. Test Setup for Cylindrical Outer Section

the results of the experiment. The small initial pulse in Figures 22 a) and b) is electrical pickup and should be ignored. In Figure 22 a), the ADP crystal output

for the setup shown in Figure 21 is given. Then the 10" long section was removed and the ADP crystal was mounted on the shaped component. The ADP crystal output for this setup is shown in Figure 22 b).

Two conclusions may be drawn from the experimental results shown in Figure 22.

1) Reflections do occur at plane C. In Figure 22 a), the first response, which is due to the direct stress wave, may be seen clearly. It is followed by a smaller but similar response roughly 150 microseconds later, which is the time required for the wave to travel from the ADP crystal end to plane C and back to the ADP crystal at the bar velocity, v_b. The later small responses are due to multiple reflections between the end and plane C. In Figure 22 b), the reflected wave follows the direct wave by only 65 microseconds. It arrives back at the ADP crystal before the crystal response from the direct pulse has ended and there is a reinforcing effect.

2) The stress wave does travel through the cylindrical outer section without any appreciable dispersion. This may be seen by comparing the ADP crystal output at the end of the cylindrical outer section due to the direct stress wave,

which is the first response of Figure 22 a), with the ADP crystal output just before it enters the transition section, which is shown in Figure 20 b).

This establishes the fact that reflections do occur at plane C of the specimen. As stated in part III E, if reflections do occur at plane C, then the elimination of the cylindrical outer section could lead to a better specimen design. This will be investigated experimentally in part IV K.

I. Stress Waves in the End Section

In part III F, it was predicted that a "δ (t) head", which is an impulsive stress wave covering an area of diameter, D_m, would travel into the end section at a velocity, v_d. This requires that, except for some small effects from reflected spherical dilatational waves, the ADP crystal on surface A of the specimen will only be excited within a circular area of diameter, D_m.

This has been verified in all of the experiments using the large specimens (L1, L2, and L3). When the entire crystal lies inside the circle of diameter, D_m, the response is independent of its exact position. If the crystal is placed so that it is at a distance halfway between the centerline and the edge of surface A, the

response is about one half as large because only 1/2 of the crystal lies inside the circle. If the crystal is placed near the edge of surface A, the response consists only of low amplitude hash because the crystal lies entirely outside of the circle.

J. Reflections at Critical Points of the Specimen

All of the reflections of the stress waves in the specimen occur at three places: surfaces A and B and planes C. The reflections at plane C were investigated experimentally in part IV H above. The reflections at surfaces B and A, which are predicted in items 5) and 6) of part III G respectively, are verified by the following experiment.

The experimental setup is identical to that used in part IV B, except that the 2" long hardened steel bar is dropped onto the 1" diameter end of the specimen shown in Figure 23. This specimen is fabricated from

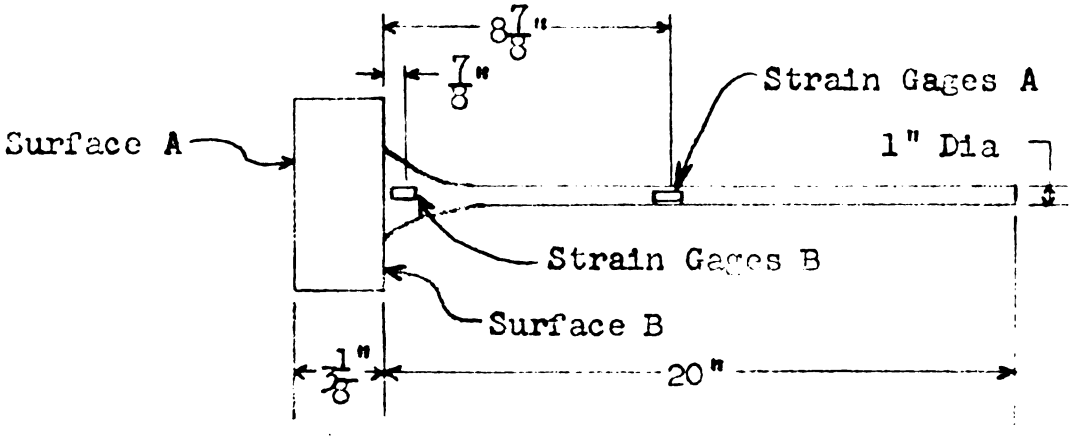

Figure 23. Reflection Test Specimen

test specimen L3 by removing one end. Obviously, this test was performed after all of the testing of the large specimens L1, L2, and L3 was completed.

Strain gages A and B are arranged in Wheatstone bridges so that bending is cancelled. The diameter at gages B is 1.7 times as large as at gages A.

The output of gages A is shown in Figure 24 a) and the output of gages B is shown on Figure 24 b).

The first pulse in Figure 24 a) is the stress wave traveling down the test section. The second pulse is the stress wave that was reflected from surface B with

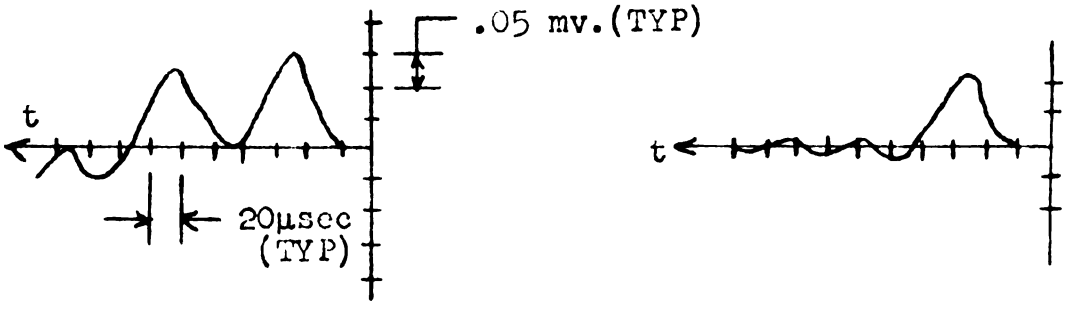

(a) Output of Gages A (b) Output of Gages B

Figure 24. Reflected Stresses in Specimen

no change of sign. Notice that it is slightly smaller than the first pulse. The third pulse is the one that was transmitted at surface B and then reflected back with a change of sign at surface A. Notice that it has a rather small amplitude as was predicted. The pulse width

of the third pulse is shortened, because a reflection from the top end of the specimen arrives at gages A before this pulse has completely passed. This verifies the reflection theories for surfaces B and A.

The first pulse in Figure 24 b) is a combination of the first and second pulse of a). They combine together, because the first pulse has traveled only 1.75 inches (or about 10 microseconds) before the second pulse arrives at gages B. The maximum amplitude of the combination of the first and second pulse of a) is 0.24 millivolts. This takes the 10 microseconds difference into account. Its amplitude in the transition section should be 1/1.7 = 0.6 as large as in the test section, because the amplitude varies as the inverse of the diameter ratio. Thus, theory predicts that this pulse should have an amplitude of 0.145. The amplitude of this pulse is found to be about 0.12. The discrepancy may be attributed to the fact that the surface of the transition section at the location of gages B makes an angle of 20 degrees with the centerline of the specimen and to experimental error. The second pulse in b) is from the reflection with a change in sign at surface A. The third pulse in b) is the wave that is reflected with a change of sign from surface A, reflected again with a change of sign from the rapid decrease of cross section at the transition section (as

was shown in part IV G), then reflected back again with a change of sign at surface A. Thus, Figure 24 b) verifies the reflection theories for surfaces A and B and plane C, as well as verifying the mode of stress wave propagation through the transition section.

K. Optimum Design of Specimen

It was predicted in part III H that the elimination of the cylindrical outer section would produce an optimum specimen design. The improvement in design was predicated because of the changes in the reflections that occur at plane C of the specimen. These reflections, which were shown to exist in part IV H, tend to "hash up" the signal.

Specimens L1, L2, and L3 were tested to determine whether shortening the cylindrical outer sections would produce a cleaner signal as predicted. The experimental setup is shown in Figures 2 and 8. The Barium Titanate input probe was located at the center of the test section in the "axial centerline position". The filters were adjusted to pass only the first subharmonic component of the ADP crystal output. A steel end cap was used at the end opposite the ADP crystal only.

The experimental results are shown in Figure 25. The results for specimens L1, L2, and L3, are given in Figures 25 a), b), and c) respectively. Notice that

the first large pulse is relatively unchanged between specimens. The small initial disturbances are electrical pickup and should be ignored. The pulses that follow are reflections from the ends of the specimen. The reflected pulses are smaller as the length of the cylindrical outer section is decreased. The ADP crystal response for specimen L3 contains a rather clearly defined large pulse of relatively short duration, followed by smaller pulses. This is an acceptable signal for acoustic emission research.

This demonstrates that the complete elimination of the cylindrical outer section, such as in specimen L3, represents an optimum specimen design.

L. Scale Effects

A half-scale version of the optimum specimen design L3, which is called specimen M1, was tested to determine whether the results obtained in these experiments are sensitive to the size of the specimen.

The experimental setup was identical to that used for specimen L3 above. The results are shown in Figure 26. The initial pulse in Figure 26 is electrical pickup and should be ignored. A comparison of Figure 26 with Figure 25 c) shows that the ADP crystal outputs are essentially the same for test specimens L3 and M1 respectively. In

both cases, there is a relatively large initial pulse followed by smaller pulses.

Thus, the use of very large specimens (types L) to accommodate a Barium Titanate input probe, which simulates the acoustic emissions, is a valid experimental technique.

M. Optimum Design of Instrumentation and Experimental Techniques

The optimum specimen design was determined in part IV K. Next, consider the question of whether the signal could be improved by changing the instrumentation or by the use of steel end caps.

Using the medium size optimum specimen design M1 and the experimental setup of part IV K, the following variations in instrumentation and experimental techniques were tried.

1) Steel end caps were used at both ends and only the first subharmonic frequency was observed. The results are shown in Figure 27 a).
2) A steel end cap was used only at the end opposite the ADP crystal and the natural frequency component of the ADP crystal output was filtered off. The results are shown in Figure 27 b).
3) Steel end caps were used at both ends and the natural frequency component of the ADP crystal was filtered off. The results are shown in Figure 27 c).

All of these methods produce a single rather large amplitude short duration pulse followed by hash signals at a lower amplitude. All of them are acceptable signals for acoustic emission research.

The choice of which of these systems is optimum rests with the investigator. He must consider the instrumentation and equipment available. However, a recommendation for the optimum system, along with arguments to justify the choice, are given in Section V.

V

CONCLUSIONS AND RECOMMENDATIONS

It may be concluded from the results of this study that it is possible to design an improved system for acoustic emission research. The system unit output is a characteristic signal that may be identified as being caused by the occurrence of one acoustic emission. This characteristic signal consists of a relatively large amplitude short duration pulse, followed by smaller "hash" pulses. The number of acoustic emissions occurring in the specimen may be determined by counting the number of characteristic pulses in the system output. Successive acoustic emissions would have to occur at a very short time interval to cause the characteristic pulses to interfere, because the width of the large pulse is about 50 microseconds.

The optimum specimen design is one which has no cylindrical outer sections. Specimen L3 and M1 are examples of this optimum design. The theoretical reasons for its being an optimum design are given in part III H. Experimental verification is given in part IV K.

Using an optimum design test specimen, there are four possible variations of experimental technique and electronic instrumentation that yield acceptable system outputs for acoustic emission research. They are:

1) Steel end cap at the end opposite the ADP crystal. Monitor only the first subharmonic frequency component of the ADP crystal output. See Figure 26.

2) Steel end caps at both ends. Monitor only the first subharmonic frequency component of the ADP crystal output. See Figure 27 a).

3) Steel end cap at the end opposite the ADP crystal. Filter off only the natural frequency component of the ADP crystal output. See Figure 27 b).

4) Steel end caps at both ends. Filter off only the natural frequency component of the ADP crystal output. See Figure 27 c).

It is recommended that the method of 1) above be used.

Methods 2) and 4) can be rejected as being inferior to 1) and 3) respectively, because the signal output is reduced by approximately one half. This is to be expected when a steel end cap is used at the ADP crystal end. The "hash" part of the signal is reduced by using the steel end cap at the ADP crystal end, but the "hash" is not as important as the signal amplitude.

It may be seen that the signal of method 3) is superior to 1), because the amplitude of the main pulse is larger and the "hash" is smaller relative to the main

pulse. However, method 3) involves instrumentation which passes a wide band of frequencies. Only extraneous noise and the natural frequency component of the ADP crystal output and above are eliminated. Method 1) involves instrumentation which passes a very narrow band of frequencies at the first subharmonic frequency component of the ADP crystal output.

In the natural acoustic emission research, the ADP crystal output that results from the acoustic emission is extremely small. At these signal levels, many extraneous signals can be of sufficient amplitude to interfere with the main signal. If a wide band of frequencies is passed by the instrumentation, there is more chance of extraneous signal interference. When only a very narrow band of frequencies is passed by the instrumentation, the chances of extraneous signal interference is very small. Method 1) would probably eliminate the necessity of testing at night. Thus, the lower signal output of method 1) is counterbalanced by the advantages just mentioned.

The amplitude of the output of method 1) can be improved by increasing the gain of the amplifier. A sharp narrow band amplifier also serves as its own filter; because it rejects all frequencies outside of its narrow band. It is possible to construct a good narrow band amplifier for the appropriate frequency by slightly altering a standard radio circuit.

If the simulated acoustic emission input used in these experiments is a good mock-up of a natural acoustic emission, then the optimum system design should be that recommended above.

The signal shown in Figure 17 is an example of the signal that would be obtained when no optimization of the system has been accomplished. Obviously, it is virtually useless for acoustic emission research. The signal in Figure 26 shows how this signal may be "cleaned up" to make it usable for acoustic emission research.

VI

BIBLIOGRAPHY

(AS 58) Aseltine, J.A. Transform Method in Linear System Analysis, McGraw-Hill, New York, 1958, pp. 24-29.

(AN 59) Ang, D.D. and Williams, M.L., "The Dynamic Stress Field due to an Extensional Dislocation", Proc. 4th Midwestern Conf. Solid Mech., Austin, Texas, U. of Texas Press, Sept. 1959, pp. 36-52.

(BA 41) Bancroft, D., "The Velocity of Longitudinal Waves in Cylindrical Bars", Phys. Rev., V. 59, 1941, pp. 588-593.

(BE 60) Bell, J. F., "The Initial Development of an Elastic Strain Pulse Propagating in a Semi-Infinite Bar", Johns Hopkins U., Nov. 1960, pp. 1-31.

(CA 59) Campbell, J. D., Simmons, J.A., and Dorn, J.E., "On the Dynamic Behaviour of a Frank-Read Source", Minerals Research Laboratory, Inst. of Engrg. Res., U. of Cal. Berkeley, Ser. 133, May 15, 1959.

(CH 39) Chree, C., "The Equations of an Isotropic Elastic Solid in Polar and Cylindrical Co-ordinates, Their Solution and Application", Proc. Camb. Phil. Soc., V. 14, 1889, p. 250.

(CO 53) Cottrell, A. H., Dislocations and Plastic Flow in Crystals, Oxford at the Clarendon Press, 1953 pp. 8-11.

(CU 60) Curtis, C.W., "Propagation of an Elastic Strain Pulse in a Semi-Infinite Bar", International Symposium of Stress Wave Propagation in Materials, Interscience Publishers, 1960, pp. 15-43.

(DA 48) Davies, R.M., "A Critical Study of the Hopkinson Pressure Bar", Phil Trans. Roy. Soc. London, Ser. A, V. 24, 1948, pp. 375-457.

(ES 49) Eshelby, J.D., "Uniformly Moving Dislocations", Proc. Phys. Soc. London, A, V. 62, 1949, pp. 307-314.

(FL 61) Flynn, P.D. and Freent, N.M., "On Saint Venant's Principle under Dynamic Conditions", Experimental Mech., S.E.S.A. Jan. 1961, pp. 15-20.

(HU 54) Huth, J.H. and Cole, J.D., "Impulsive Loading on an Elastic Half-Space", J. Appli. Mech., V. 21, No. 3, Sept. 1954, pp. 294-295.

(JO 59) Johnston, W. G. and Gilman, J. J., "Dislocation Velocities, Dislocation Densities, and Plastic Flow in Lithium Fluoride Crystals", J. Appli. Phys., V. 30, No. 2, Feb. 1959, pp. 129-144.

(KA 50) Kaiser, J., "Untersuchungen uber das Auftreten von Gerauschen biem Zugversuch", Ph.D. Thesis, Techn. Hochsch., Munchen, 1950.

(KO 54) Kolsky, H., "The Propagation of Longitudinal Elastic Waves along Cylindrical Bars", Phil. Mag., 7th Ser., V. 45, No. 360, 1954, pp. 712-726.

(LE 59) Lessells and Associates, Inc., "Acoustic Emission Under Applied Stress", Progress Reports 4 and 5, WADC Contract No. AF 33(616)-5640, 1959.

(LI 60) Lindsay, R.B., Mechanical Radiation, McGraw-Hill, New York, 1960, pp. 74-78.

(MA 51) Mason, W. P. and Wick, R.F., "A Barium Titanate Transducer Capable of Large Motion at an Ultrasonic Frequency", J. Acoust. Soc. Amer., V. 23, No. 2, March 1951, pp. 209-214.

(MC 61) McNiven, H.D., "Extensional Waves in a Semi-Infinite Elastic Rod", J. Acoust. Soc. Amer., V. 33, No. 1, Jan. 1961, pp. 23-27.

(MI 51) Mindlin, R.D. and Herrmann, G., "A One-Dimensional Theory of Compressional Waves in an Elastic Rod", Proc. 1st. U.S. Natl. Cong. Appl. Mech., A.S.M.E., June 1951, 1952, pp. 187-191.

(MI 56) Miklowitz, J., "The Propagation of Compressional Elastic Waves along Cylindrical Bars", Phil. Mag., 7th Ser., V. 45, No. 366, 1954, pp. 712-726.

(NA 47) Nabarro, F.R.N., "Dislocations in a Simple Cubic Lattice", Proc. Phys. Soc., V. 59, 1947, pp. 256-272.

(OL 57) Oliver, J., "Elastic Wave Dispersion in a Cylindrical Rod by a Wide-Band Short-Duration Pulse Technique", J. Acoust. Soc. Amer., V. 29, No.2, Feb. 1957, pp. 189-194.

(OR 34) Orowan, E., "Zur Kristallplastizitat, Part III Uber den Mechanismus des Gleitvorganges", Z. Physik, V. 84, 1934, pp. 634-659.

(PE 40) Peierls, R., "The Size of a Dislocation", Proc. Phys. Soc., V. 52, 1940, pp. 34-37.

(PO 76) Pockhammer, L. "Ueber die Fortpflanzungsgeschwindigkeit kleiner Schwingungen in einem unbegrenzten isotropen Kreiscylinder", J. reine u. angew. Math., V. 81, 1876, p. 324.

(RI 57) Ripperger, E.A. and Abramson, H.N., "Reflection and Transmission of Elastic Pulses in a Bar at a Discontinuity in Cross Section", Proc. 3rd. Midwestern Conf. Solid Mech., Ann Arbor, Michigan Press, April 1957, pp. 135-145.

(SC 58) Schofield, B.H., Bareiss, R.A., and Kysala, A.A., "Acoustic Emission Under Applied Stress", WADC Tech. Rep. 58-194, ASTIA Doc. No. AD 155 674, April 30, 1958.

(TA 34) Taylor, G.I., "The Mechanism of Plastic Deformation of Crystals", Proc. Roy. Soc. London, V. 145, Ser. A, 1934, pp. 362-404.

(TI 55) Timoshenko, S., Vibration Problems in Engineering, D. Van Nostrand Co., Inc., New York, 1955, pp. 76-86.

(WO 61) Wolkowisky, J. H., "Attenuation of Sound in Some Overloaded Absorbers by a Pulse Technique", M.S. Thesis, Michigan State University, East Lansing, 1961.

FIGURES

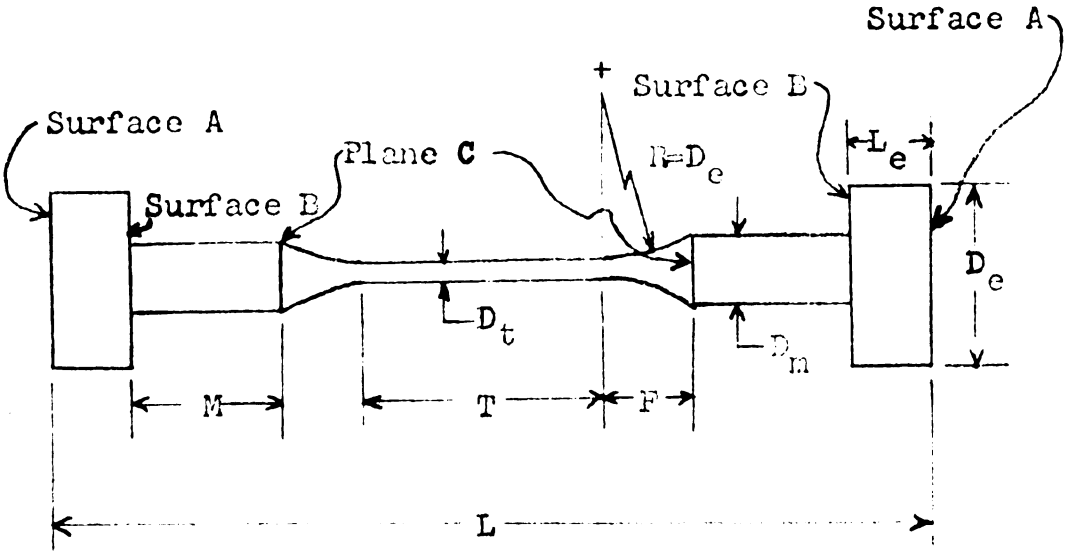

Specimen Designation	D_e=R	D_m	D_t	F	L	L_e	M	T
S1	1.0	.50	.2	.527	6.55	.875	1.50	.750
M1	2.5	1.25	.5	1.317	15.14	1.563	0	9.375
L1	5.0	2.50	1.0	2.635	30.27	3.125	7.50	3.750
L2	5.0	2.50	1.0	2.635	30.27	3.125	3.75	11.250
L3	5.0	2.50	1.0	2.635	30.27	3.125	0	18.750

Notes 1) All dimensions are inches.

2) All specimens are fabricated from 2024 aluminum bar.

3) In specimen designations: S = small, M = medium, L = large.

4) In dimensions: D = diameter, R = radius, L_e = length of end section, F = length of transition section, L = specimen length, M = length of section between the end section and transition section, T = length of test section.

Figure 1. Geometry of the Test Specimens

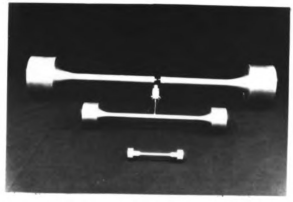

Figure 3. The Large, Medium and Small Size Test Specimens

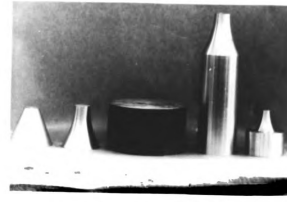

Figure 4. Separate Components of the Test Specimens

Figure 5. Barium Titanate Input Probe

Figure 7. ADP Crystal and General Radio Amplifier

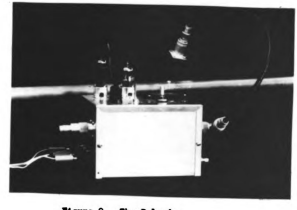

Figure 9. The Pulsed Oscillator

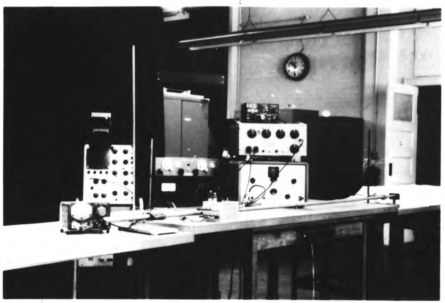

Figure 6. Experimental Setup for Frequency Response Tests

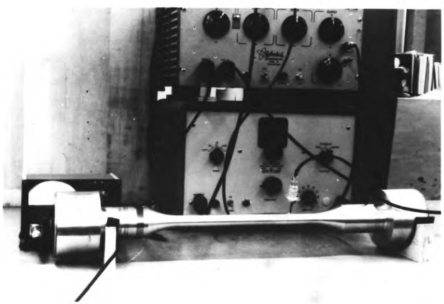

Figure 8. Part of the Experimental Setup for Test Specimens

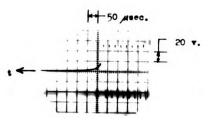

(a) Pulsed Oscillator Output

(b) ADP Crystal Response

Figure 13. Oscilloscope Records of Frequency Response Tests

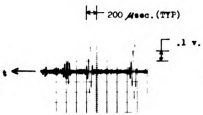

(a) No Steel End Cap

(b) With Steel End Cap

Figure 20. Effect of the Steel End Cap

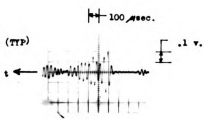

(a) With 10" Long Cylinder

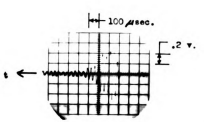

(b) Without 10" Long Cylinder

Figure 22. Stress Waves in the Cylindrical Outer Section

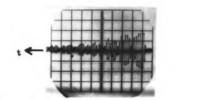

(a) Specimen L1

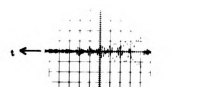

(b) Specimen L2

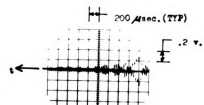

(c) Specimen L3

Figure 25. Comparison of ADP Crystal Output for Specimens L1, L2, L3

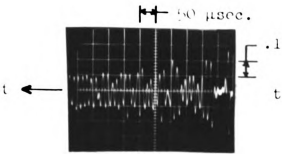

Figure 17.
ADP Output Signal
before "Cleaning Up"

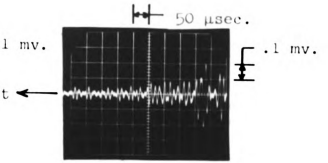

Figure 20.
ADP Crystal Output
for Specimen M1

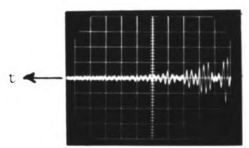

(a) Method 1

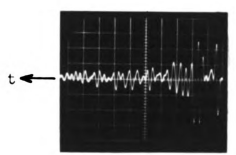

(b) Method 2

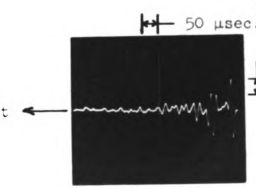

(c) Method 3

Figure 21. ADP Crystal Output for Various Instrumentation and Experimental Technique Methods

APPENDIX A

Propagation of $\delta(t)$ Type of Impulsive Stress Wave through a Transition Section

The transition section, taken as a separate component, is shown in Figure A1.

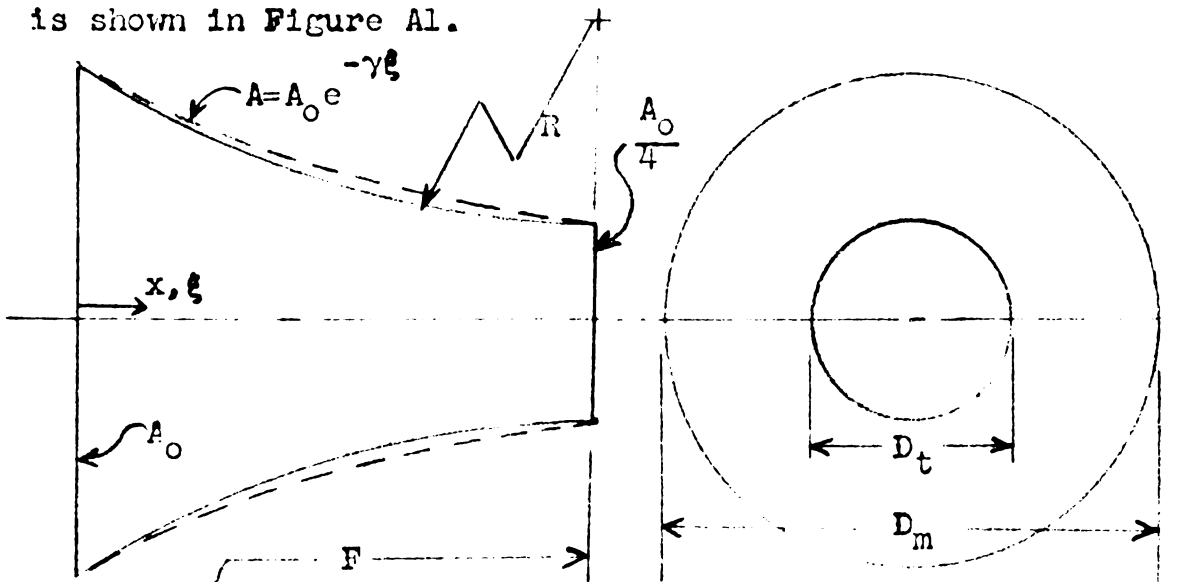

Figure A1. Geometry of the Transition Section

Assume that the stress is purely extensional and is uniform across the cross section. Let

$$\xi = x/F \qquad (1)$$

A free body diagram of a differential length, $Fd\xi$, of the transition section is shown in Figure A2. An equilibrium equation for the ξ direction is obtained from the free body diagram of Figure A2.

$$\sigma \frac{dA}{d\xi} + A\frac{\partial \sigma}{\partial \xi} = \rho AF \frac{\partial^2 u}{\partial t^2} \qquad (2)$$

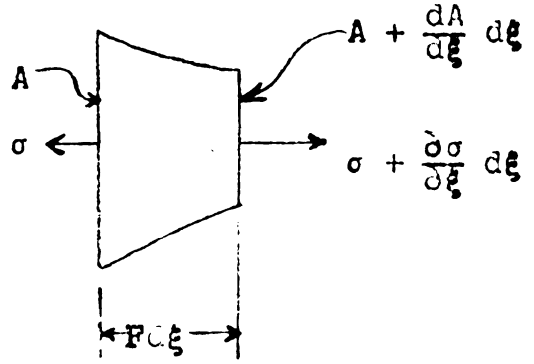

Figure A2. Free Body Diagram of an Element of the Transition Section

The stress is given in terms of u as

$$\sigma = E \frac{\partial u}{\partial x} = \frac{E}{F} \frac{\partial u}{\partial \xi} \qquad (3)$$

Substitute (3) into (2).

$$\frac{\partial^2 u}{\partial \xi^2} + \frac{1}{A} \frac{dA}{d\xi} \frac{\partial u}{\partial \xi} = \frac{\rho F^2}{E} \frac{\partial^2 u}{\partial t^2} \qquad (4)$$

The solution of equation (4) is complicated by the fact that the coefficient of $\frac{\partial u}{\partial \xi}$ is in general a function of ξ. However, if the transition section has the form of an exponential horn,

$$A = A_o e^{-\gamma \xi} \qquad (5)$$

then

$$\frac{1}{A} \frac{dA}{d\xi} = -\gamma \qquad (6)$$

and equation (4) becomes

$$\frac{\partial^2 u}{\partial \xi^2} - \gamma \frac{\partial u}{\partial \xi} = \frac{\rho F^2}{E} \frac{\partial^2 u}{\partial t^2} \qquad (7)$$

Equation (7) is much simpler than equation (4). The shape of the exponential horn is shown dotted in Figure A1. The analysis of the exponential horn will be considered to be valid for the actual transition section, because of the similarity of the shapes.

The stress wave introduced into the transition section is a $\delta(t)$ type of impulsive stress wave, traveling at velocity, v_b. Assume that the stress wave remains impulsive and travels through the transition section at the bar velocity, v_b, but changes amplitude. This is represented by the following displacement function

$$u(\xi, t) = U(\xi)\delta(t - \frac{\xi F}{v_b}) \qquad (8)$$

Equation (8) is substituted into equation (7).

$$-\frac{2F}{v_b} U'\delta' + \frac{F^2}{v_b{}^2} U\delta'' + U''\delta + \frac{F\gamma}{v_b} U\delta' - \gamma U'\delta = \frac{\rho F^2}{E} U\delta'' \qquad (9)$$

The second term on the left cancels with the term on the right hand side, because $v_b{}^2 = \frac{E}{\rho}$. This shows the necessity of the assumption that the stress wave travels through the transition section at velocity, v_b. Equation (9) now becomes

$$\frac{F}{v_b} \frac{2U' - \gamma U}{U'' - \gamma U'} = \frac{\delta}{\delta t} \qquad (10)$$

where the primes on U refer to differentiation with respect to ξ. The prime on δ refers to differentiation with respect to $(t - \frac{\xi F}{v_b})$, but it can also be interpreted as meaning differentiation with respect to t, because

$$\frac{\partial}{\partial t} = \frac{\partial}{\partial(t - \frac{\xi F}{v_b})} .$$

The quantity δ/δ' can be constructed by noting that for $\varepsilon \to 0$, we have δ represented by Figure A3 and δ' represented by Figure A4 (AS 58).

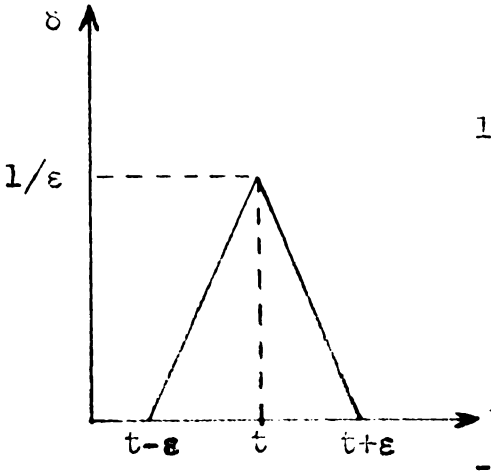

Figure A3. $\delta(t)$

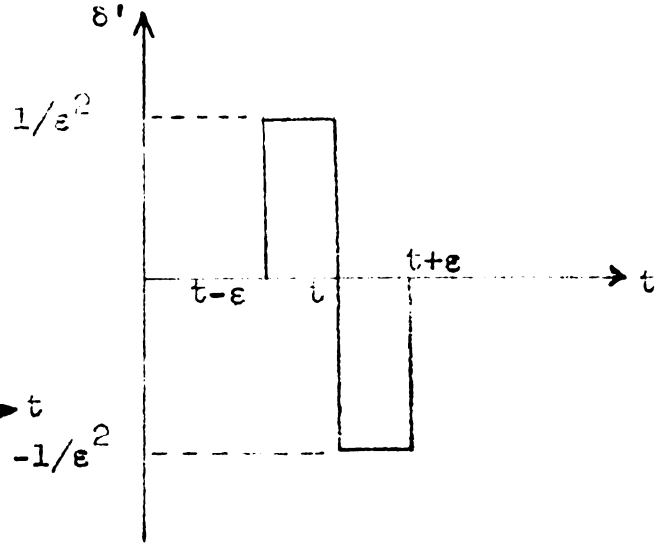

Figure A4. $\delta'(t)$

Then the quantity δ/δ' is given by Figure A5.

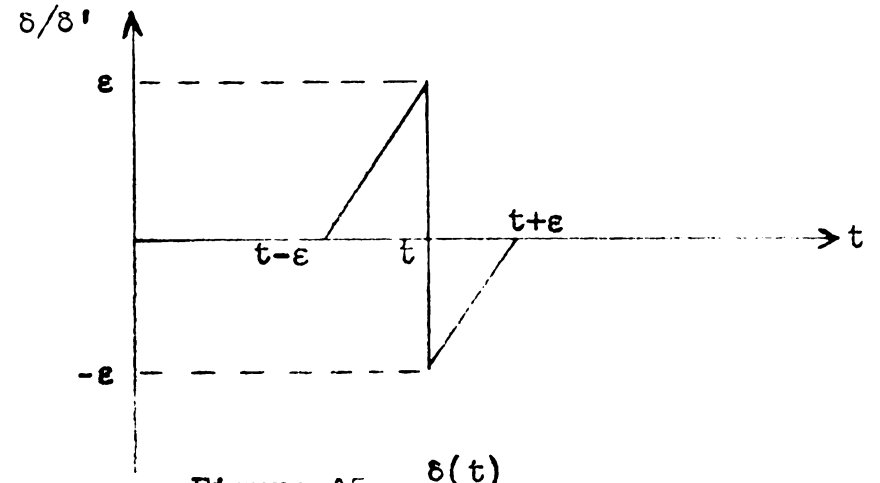

Figure A5. $\frac{\delta(t)}{\delta'(t)}$

Obviously, as $\varepsilon \to 0$, $\delta/\delta' \to 0$.

Then equation (10) becomes

$$\frac{F}{v_b} \frac{2U'-\gamma U}{U''-\gamma U'} = 0 \qquad (11)$$

Thus $$2U' - \gamma U = 0 \qquad (12)$$

The solution of (12) is

$$U = u_o e^{\frac{\gamma \xi}{2}} \qquad (13)$$

Substitute (13) into (8) and get

$$u(\xi,t) = u_o e^{\frac{\gamma \xi}{2}} \delta(t - \frac{\xi F}{v_b}) \qquad (14)$$

An expression having the form of equation (8) was assumed for the solution of differential equation (7). When this expression was substituted into the differen-

tial equation, equation (14) resulted. Equation (14) is a solution of differential equation (7), as may be checked by direct substitution. Therefore, the assumptions, which led to equation (8), are valid.

From equations (3) and (14) we get

$$\sigma = \frac{Eu_o}{F} e^{\frac{\gamma\xi}{2}} \delta(t - \frac{\xi F}{v_b}) \left[\frac{\gamma}{2} - \frac{F}{v_b} \frac{\delta'(t - \frac{\xi F}{v_b})}{\delta(t - \frac{\xi F}{v_b})} \right] \tag{15}$$

Again, using $\delta/\delta' \to 0$ as $\varepsilon \to 0$, equation (15) becomes

$$\sigma = \frac{Eu_o\gamma}{2F} e^{\frac{\gamma\xi}{2}} \delta(t - \frac{\xi F}{v_b}) \tag{16}$$

Since $\varepsilon = \sigma/E$

$$\varepsilon = \frac{u_o\gamma}{2F} e^{\frac{\gamma\xi}{2}} \delta(t - \frac{\xi F}{v_b}) \tag{17}$$

Denoting the conditions at $\xi = 0$ by the subscript "o", equations (16) and (17) may be written as

$$\frac{\sigma}{\sigma_o} = e^{\frac{\gamma\xi}{2}} \tag{18}$$

$$\frac{\varepsilon}{\varepsilon_o} = e^{\frac{\gamma\xi}{2}} \tag{19}$$

It should be understood that equation (18) is the ratio of the amplitude of the stress wave as it passes through point ξ divided by the amplitude of the stress wave when

it passed through point $\xi = 0$. These are not at the same time. The same remarks apply to equation (19).

Since

$$\frac{A}{A_o} = e^{-\gamma\xi} \tag{5}$$

then, $$\frac{D}{D_o} = e^{-\frac{\gamma\xi}{2}} \tag{20}$$

Substitution of (20) into (13) and (19) yields

$$\frac{\sigma}{\sigma_o} = \frac{D_o}{D} \tag{21}$$

$$\frac{\varepsilon}{\varepsilon_o} = \frac{D_o}{D} \tag{22}$$

Therefore, both the stress and strain vary as the inverse of the diameter ratio. Macon (MA 51) solved the problem of the propagation of sinusoidal stress waves through an exponential horn and found the same variation of stress and strain.

APPENDIX B

Stress Wave Propagation in a Half-Space with an Impulsive δ(t) Load on a Circular Area of the Surface

Huth and Cole (HU 54) have analyzed the problem of a half-space with a unit-step function type of impulsive load, u(t), distributed uniformly over a circular area of the surface. The load is zero for $t < 0$ and of unit amplitude (pounds per square inch) for $t > 0$.

The results of their analysis are shown in Figure B1. Region I is stress free. Region II has a uniform unit

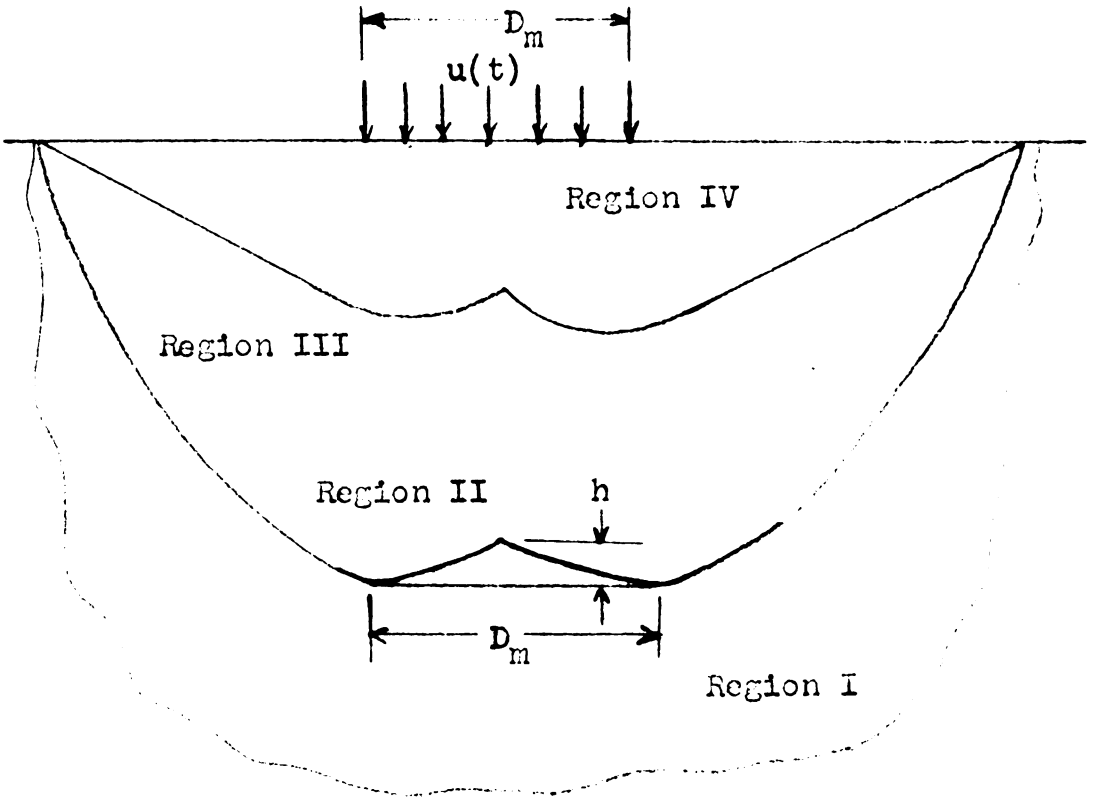

Figure B1. Stress Waves due to a Unit-Step Function Impulsive Loading

amplitude extensional stress. Region III has a dilatational spherical stress whose amplitude varies approximately inversely proportional to the spherical radius. Region IV contains both dilatational and shear stress. Since we are not interested in shear stress waves, because the ADP crystal reacts to normal stresses only, we will not be interested in the distinction between regions III and IV.

Region II is the interesting part of the stress wave propagation. Huth and Cole call this region the "head". From the geometry of Figure B1, it is seen that the diameter of the "head" is always D_m, which is the same as the applied load diameter. Therefore, a "head" of uniform extensional stress of the same diameter and amplitude as the applied load penetrates into the half-space. The height, h, of the "head" varies inversely proportional to the penetration distance squared. Therefore, the "head" becomes thin with any appreciable penetration distance.

Since the amplitude of the dilatational stress in Region III-IV is approximately inversely proportional to the spherical radius, the stresses in this region become small with appreciable penetration distance.

Huth and Cole used a unit-step function type of impulsive load, u(t). However, the stress wave introduced into the end section of the specimen will be very close to the $\delta(t)$ type of impulsive load.

The following relationship (AE 50) exists between $\delta(t)$ and $u(t)$.

$$\delta(t) = \frac{du(t)}{dt} \qquad (1)$$

Since the impulsive load in the end section is the time derivative of the impulsive load of Huth and Cole, then the stress wave propagation in the end section should be the time derivative of the stress wave propagation of Huth and Cole. The question of the differentiability of Huth and Cole's solution can be raised. This question will not be answered analytically. The agreement between experimental results and the theory will serve to establish the validity of this approach.

Neglecting the difference between Regions III and IV, it is seen that, during any small increment of time, the only time varying part of the stress wave propagation of Huth and Cole occurs at the "head" and along the spherical dilatation wave front of Region III.

At any significant penetration distance, the strength of the spherical dilatation front is small. Therefore, as the front passes a point in the body, the stress changes instantly from the zero of Region I to a small value of Region III and remains constant. The time derivative of the passage of the spherical dilatation front through a point corresponds to a weak $\delta(t)$ type of

impulsive stress wave. This will be considered to be a second order effect.

Now, consider a point which is in the path of the "head" as it penetrates into the body. The stress changes instantly from the zero of Region I to the unit amplitude of the "head". The "head" is thin and, therefore, the stress remains at unit amplitude for only the short time required for the "head"to pass by the point. Then the stress drops to a small value in Region III and remains constant. The time derivative of the passage of the "head" through a point is, therefore, a $\delta(t)$ type of impulsive stress wave. The amplitude of this stress wave is much larger than that of the wave associated with Region III for any significant penetration distance.

Therefore, for a $\delta(t)$ type of impulsive loading, the stress wave propagation consists primarily of a large amplitude $\delta(t)$ type of impulsive stress wave, having the same diameter as the load, traveling into the half-space with a velocity, v_d. For brevity, this will be called the "$\delta(t)$ head". Small amplitude $\delta(t)$ type spherical wave fronts, traveling with a velocity, v_d, also exist.

APPENDIX C

List of Electronic Equipment Used in this Investigation

Reference Code	Description of Equipment
A	Low Frequency Function Generator, Model 202A, Hewlett Packard Co., Palo Alto, Calif.
B	Pulse Generator, Model B7, Rutherford Electronics Co., Culver City, California.
C	Unit Pulse Amplifier, Type No. 1219-A, General Radio Co., Cambridge, Massachusetts.
D	Tuned Amplifier and Null Detector, Type 1232-A, General Radio Co., Concord, Massachusetts.
E	Variable Electronic Filter, Model 302, Spencer-Kennedy Laboratories, Boston, Massachusetts.
F	Variable Electronic Filter, Model 3081, Spencer-Kennedy Laboratories, Inc.
G	Tektronix Oscilloscope, Type 532, Tektronix Inc., Portland, Oregon.
G1	Type 53/54D Plug-In Unit, Tektronix Inc.
G2	Type 53/54E Plug-In Unit, Tektronix Inc.
H	Oscillograph Record Camera, Type 2620, Allen B. Du Mont Laboratories Inc., Clifton, N. J.
J	Pulsed Oscillator, designed and assembled for this project at Michigan State University, See Section II G and Figure 11.